Robust Beamforming Design for RSMA-Integrated Full-Duplex Communications: Energy and Spectral Efficiency Trade-off

Raviteja Allu, Mayur Katwe, *Member, IEEE*, Keshav Singh, *Member, IEEE*, Simon L. Cotton, *Senior Member, IEEE*, Chih-Peng Li, *Fellow, IEEE*, and Trung Q. Duong, *Fellow, IEEE*

***Abstract*—In this paper, we investigate an unconventional full-duplex (FD) integrated rate-splitting multiple access (RSMA) scheme for improved spectral efficiency (SE) and energy efficiency (EE) performance when compared to the conventional power-domain schemes. In particular, we focus on improving the energy efficiency (EE) and spectral efficiency (SE) trade-off for the multiple users subject to robust beamforming design and smart inter-user interference mitigation under imperfect channel state information (CSI). We formulate a multi-objective optimization (MOO) problem, specifically aiming to jointly maximize EE and SE within the FD-RSMA system by jointly optimizing the resource allocation subject to the limits on transmit power and minimum rate, under the assumption of a CSI error model with a bound. Initially, the MOO problem is converted into a single objective optimization (SOO) problem using the weighted sum method, with a trade-off parameter. An iterative algorithm is employed, utilizing successive convex approximation and the S-procedure to achieve near-optimal resource allocation for the transformed SOO problem, with a particular emphasis on effective interference management. Simulation results highlight the effectiveness of the FD-RSMA scheme, demonstrating its superiority over the multi-user FD space division multiple access by 16.93 % and non-orthogonal multiple access scheme by 76.04 %.**

***Index Terms*—Energy efficiency, full-duplex, rate-splitting multiple access technique, robust beamforming, SE-EE trade-off, spectral efficiency.**

I. Introduction

THE advent of sixth generation (6G) networks heralds transformative advancements in wireless communication technology. Within the context of 6G, the critical roles of spectral efficiency (SE) and energy efficiency (EE) are further accentuated due to the increasing demands and complexities of modern connectivity [1]. As 6G aims to support vast data volumes and ultra-high-definition media, SE becomes crucial for meeting the escalating need for rapid and seamless connectivity. Simultaneously, EE emerges as a pivotal concern in the evolution of 6G, driven by the necessity for sustainable and environmentally friendly technologies [2]. Nevertheless, the stringent power limitations inherent in 6G networks necessitate sophisticated optimization techniques that balance high data throughput with minimal energy consumption. The inherent trade-off between SE and EE is a central challenge in the design of wireless communication systems. A crucial approach to addressing this balance is through the maximization of resource efficiency (RE), a performance metric designed to flexibly and effectively harmonize SE and EE [3], [4]. By focusing on RE, 6G networks can achieve an optimal trade-off, ensuring efficient resource use and the adoption of sustainable technology without sacrificing data rates or energy efficiency.

In the pursuit of maximizing network performance, significant strides can be made through the adoption of innovative physical layer techniques such as full-duplex (FD) [5] and rate-splitting multiple access (RSMA) [6]–[9] schemes. FD technology enables simultaneous transmission and reception over the same frequency band, effectively doubling spectral efficiency and optimizing spectrum utilization [5]. Likewise, RSMA strategically allocates resources using power-domain multiplexing, allowing for the concurrent transmission of multiple data streams to different users [10], [11]. By integrating FD and RSMA methodologies, 6G networks can achieve notable improvements in RE, striking an optimal balance between spectral and energy efficiency while meeting the ever-growing demands for high-speed data transmission in contemporary wireless communication systems. This complex interaction introduces a fresh level of efficiency, adaptability, and capacity to 6G wireless communication systems, positioned to address and surpass the requirements of an increasingly interconnected global landscape. Consequently, the careful integration of RSMA and FD emerges as essential for the 6G wireless communication model. This fusion does not simply provide marginal advantages; it fundamentally transforms the operational landscape of wireless systems. The collective potential of these technologies envisions a wireless environment where spectral and energy efficiencies are not conflicting but instead work together to forge a groundbreaking, robust, and

The work of K. Singh and C.-P. Li was supported in part by the National Science and Technology Council of Taiwan under Grant NSTC 113-2218-E-110-008, Grant NSTC 112-2221-E-110-029-MY3, and in part by the Sixth Generation Communication and Sensing Research Center funded by the Higher Education SPROUT Project, the Ministry of Education of Taiwan. The work of T. Q. Duong was supported in part by the Canada Excellence Research Chair (CERC) Program CERC-2022-00109. (*Corresponding author: Keshav Singh*.)

R. Allu, K. Singh, and C.P. Li are with the Institute of Communications Engineering, National Sun Yat-sen University, Kaohsiung 804, Taiwan (E-mail: {alluraviteja202}@gmail.com, keshav.singh@mail.nsysu.edu.tw, cpli@faculty.nsysu.edu.tw).

M. Katwe is with the Department of Electronics and Communication Engineering, National Institute of Technology Raipur, 492010, Chhattisgarh, India. (E-mail: mvkatwe.ece@nitrr.ac.in).

S. L. Cotton is with the Centre for Wireless Innovation, School of Electronics, Electrical Engineering and Computer Science, Queen's University Belfast, Belfast, U.K. (E-mail: simon.cotton@qub.ac.uk).

T. Q. Duong is with the Faculty of Engineering and Applied Science, Memorial University, St. John's, NL A1C 5S7, Canada, and is also with the Centre for Wireless Innovation, School of Electronics, Electrical Engineering and Computer Science, Queen's University Belfast, Belfast, U.K. (E-mail: tduong@mun.ca).

comprehensive 6G communication infrastructure.

A. Background

In the existing literature, numerous authors have extensively examined the significance of FD communication in resource allocation. Studies such as [12]–[22] have explored various aspects of FD technology, focusing on its impact on network performance. Specifically, works like [12], [14], [15] have delved into SEM problems in FD communication systems by addressing interference and proposing advanced optimization techniques, these studies contribute to significant improvements in SEM. Conversely, other researchers have concentrated on EEM within FD systems, as detailed in [16]–[19]. These works focus on reducing energy consumption while maintaining high data throughput, an essential consideration for sustainable wireless communication networks. Moreover, the literature on RSMA has also seen significant contributions concerning resource allocation dynamics. Key studies such as [23]–[32] have explored various facets of RSMA, focusing on its potential to improve network performance. In particular, research works like [26]–[29] have concentrated on SEM within RSMA frameworks. In addition, studies such as [30], [31] address the EEM problem within RSMA systems.

In literature, the SE-EE trade-off problem is addressed in many existing works [20]–[22], [32]–[40]. A notable contribution is presented in [33], where the authors tackled the SE-EE trade-off problem by formulating the multi-objective optimization (MOO) and reformulated the original MOO problem as a conventional single objective optimization (SOO) problem using a weighted sum approach. This method allowed them to achieve a Pareto-optimal solution, demonstrating the effectiveness of their proposed algorithm over existing beamforming designs. The scalarization method is utilized to transform the MOO problem into the SOO problem by using a function normalization process to regard EE and SE as quantities without an associated physical unit so that EE and SE are comparable to be integrated into a utility function in [35]. In [36], authors addressed the adopted ϵ-constraint method and the strict robustness to convert the MOO problem to the SOO problem considering the imperfect CSI. In [37], the robust SE-EE trade-off problem is addressed by maximizing the RE. Several studies have focused on the SE-EE trade-off problem specifically within FD systems. In [20], [21], the authors formulated the SE-EE trade-off problem by aiming to maximize system EE for a given system SE. They derived the necessary conditions under which an FD transceiver could achieve a better EE-SE trade-off compared to a half-duplex (HD) transceiver, considering different residual self-interference (RSI) models. In [41], the MOO of the SE-EE trade-off problem is addressed using the RE maximization technique. The work in [22] approached the SE-EE trade-off problem by maximizing the power-normalized signal-to-interference-plus-noise ratio (PN-SINR), providing another perspective on balancing SE and EE in FD systems. Additionally, in [38], the authors addressed the SE-EE trade-off by focusing on resource efficiency (RE) maximization and examined the joint effects of RSI and co-channel interference (CCI) on the SE-EE trade-off in reconfigurable intelligent surface (RIS)-aided FD multiple-input multiple-output (MIMO) systems. The authors in [42], adopted the utility function method in which a constant is introduced for the objective function for the selection between the SE and EE. Moreover, the SE-EE trade-off problem in RSMA-aided systems is discussed in [32], [39]. In [32], the authors transformed the separate SE and EE maximization problems into a single equivalent optimization problem. They compared the performance of RSMA against non-orthogonal multiple access (NOMA) and multi-user linear precoding (MU-LP), demonstrating that RSMA offers significant improvements in both SE and EE. In [39], the authors adopted two distinct approaches to convert the MOO problem into an SOO problem: the weighted-sum approach and the weighted-power approach. They derived closed-form solutions for each SOO problem in a two-user system and found that RSMA outperforms conventional space-division multiple access (SDMA) and NOMA in terms of both EE and SE. In [40], authors addressed the robust SE-EE trade-off by adopting RE maximization.

B. Interplay of FD and RSMA

The interplay between FD and RSMA is critical for next-generation wireless communication networks because of the following advantages.

- FD systems enable simultaneous transmission and reception over the same frequency band, thereby doubling spectral utilization. However, one of the key challenges with FD is managing self-interference (SI), especially in uplink (UL) scenarios where the user equipment typically transmits at lower power compared to the base station (BS). In this context, RSMA plays a pivotal role in mitigating SI. By allowing the BS to transmit common messages at lower rates, RSMA significantly reduces the SI in the UL. Once the common interference is handled, the BS can transmit private messages at higher rates, maximizing the overall SE. This coordinated interplay between FD and RSMA improves SE by allowing efficient handling of SI while ensuring high-rate private message delivery.
- FD naturally supports scalability by accommodating more users simultaneously due to its ability to handle both UL and DL on the same resource. When combined with RSMA, which dynamically adapts to varying channel conditions, this approach further enhances the throughput and fairness of the system. RSMA adjusts the allocation of resources between users based on their specific channel states, enabling optimal use of the available spectrum. This dynamic adaptation ensures that FD-RSMA systems can operate efficiently even in highly dense networks, where user demand and network conditions vary frequently.
- The combination of FD and RSMA also improves EE. In FD systems, the ability to transmit and receive on the same channel eliminates the need for separate UL and DL channels, thereby reducing resource usage and energy consumption. RSMA complements this by optimizing

power allocation between common and private messages. By dynamically adjusting the power levels according to the interference and channel conditions, RSMA ensures that power is used efficiently, further improving the overall EE of the communication system. This makes the FD-RSMA combination ideal for networks that need to balance high performance with low power consumption.

- RSMA's inherent robustness to imperfect CSI makes the combined FD-RSMA system highly resilient to errors in channel estimation. RSMA splits messages into common and private parts, allowing the system to handle inaccuracies in CSI without significantly degrading performance. This robustness ensures that the system can maintain high throughput and reliability even when accurate channel knowledge is not available, which is a common issue in practical wireless networks.

The integration of FD and RSMA is highly relevant in addressing real-world challenges in modern communication networks. For instance, in ultra-dense networks (UDNs) such as those deployed in smart cities or massive IoT applications, achieving high SE and EE is essential to meet the increasing demand for data and device connectivity. Traditional methods often struggle with the complexity of balancing these metrics effectively. Furthermore, this integration finds critical applications in various advanced wireless scenarios like remote patient monitoring (RPM), autonomous vehicles, smart grid communications, industrial IoT, augmented reality (AR), tactical military communications, etc. For example, in RPM timely data transmission can be life-saving. The full-duplex capability allows simultaneous UL and DL transmissions, ensuring that vital health data from patient sensors is sent in real-time while receiving critical instructions or updates from healthcare providers without delay. In the UL, RSMA enables splitting patient data into multiple sub-messages, which are then transmitted efficiently across the available spectrum. This ensures critical information is prioritized and delivered swiftly, even in congested network environments. Common signals broadcast essential health information, such as alerts or general updates, to all relevant devices or medical personnel, ensuring coordinated and rapid responses. Meanwhile, private signals securely transmit patient-specific data, safeguarding privacy and enabling personalized care. This seamless, bidirectional communication, enhanced by the granularity of sub-messages in the UL, significantly boosts the efficiency and reliability of RPM systems, leading to improved patient outcomes. However, managing cross-interference, a significant challenge in FD transmission, necessitates careful resource allocation and interference mitigation in the FD-RSMA system to optimize energy and spectral efficiency, motivating our research.

C. Motivation and contribution

Despite its advantages, the FD-RSMA system remains relatively under-explored. In previous studies [43], a cooperative RSMA scheme designated the strongest user as an FD relay for DL transmission but did not fully exploit RSMA operations for UL and DL transmission at the BS. Moreover, since EE and SE can potentially conflict with each other meaning that optimizing resources for one often comes at the expense of the other, it is essential to investigate the tradeoff between EE and SE in the FD-RSMA system. This analysis will provide decision-makers with a comprehensive performance envelope for both metrics. Importantly, our previous study on FD-RSMA [44] assumed the availability of perfect CSI, an assumption not feasible in practical scenarios. Given the random nature of wireless channels, limited channel capacity, transmission delays, and inaccuracies in channel estimation, CSI inevitably contains errors, which can significantly degrade system performance. Providing a robust optimal resource allocation strategy for addressing the SE-EE tradeoff in FD-RSMA systems is highly challenging due to several factors. These include imperfect CSI and the complex coupling of variables between the UL and DL scenarios along the RSMA strategy. The complex relationship between power allocation, beamforming, and rate-splitting variables further complicates finding an optimal solution. The presence of imperfect CSI adds another layer of complexity to the problem [45]. Robust beamforming and resource allocation need to be designed to account for norm-bounded channel estimation errors, making the problem more challenging to solve in practice. and co-channel interference (CCI). Therefore, the primary challenge is to achieve optimal power control in the FD-RSMA system, which requires sophisticated resource allocation and intelligent interference mitigation. Our work is pioneering in investigating an RSMA-integrated FD system to develop a robust, spectral, and energy-efficient multi-user communication system. To highlight the uniqueness of our study, a brief comparison with existing works in the literature is provided in Table I.

TABLE I: Comparison of our work with existing literature.

	FD	**RSMA**	**Imperfect CSI**	**Description of EE-SE trade-off problem**
[20]	✓	X	X	Maximize EE for a given SE
[21]	✓	X	X	Maximize EE for a given SE
[32]	X	✓	X	RE maximization
[33], [34]	X	X	X	RE maximization
[35]	X	X	X	Scalarization method
[36]	X	X	✓	ϵ-constraint method
[37]	X	X	✓	RE maximization
[38]	✓	X	X	PN-SINR
[39]	X	✓	X	Weighted-sum approach and Weighted-power approach.
[40]	X	✓	✓	RE maximization
[41]	✓	X	X	RE maximization
[42]	✓	X	✓	Utility function method
Our Work	✓	✓	✓	RE maximization

The primary contributions of our study are outlined below:

1) Unlike existing works, which either focus on FD or RSMA, we analyze an FD-integrated RSMA system where a BS communicates with multiple single-antenna UL and DL users concurrently in the same time and frequency slot using RSMA. To the best of the authors' knowledge, this study marks the first investigation of the FD-aided RSMA system under imperfect CSI.
2) Subsequently, we focus on RE maximization and formulate a robust multi-objective optimization (MOO) problem subject to constraints on transmit power and rate

requirements, considering bounded CSI. To solve this problem efficiently, we transform it into an equivalent single-objective optimization (SOO) problem and employ a generalized S-procedure to handle semi-infinite inequalities and successive convex approximation (SCA) to solve it.

3) Finally, we validate the computational complexity and the relative performance improvement of the proposed FD-RSMA system compared to conventional schemes through numerical simulations, considering various network parameters. Our simulation results affirm the superior performance of the FD-RSMA system compared to multi-user FD SDMA and NOMA schemes.

Structure of the paper:

The considered framework of multi-user RSMA-assisted FD communications is introduced in Section II. In Section, III, the problem formulation and proposed solution for the considered network are discussed. The results of some simulations obtained using the proposed algorithms are depicted and discussed in Section IV. Lastly, Section V finishes the paper with some concluding remarks.

Notations:

The list of notations used in this paper is given in Table II.

TABLE II: List of notations.

$\mathbf{I}_m$	Identity matrix
$\mathcal{CN}(\mathbf{0},\mathbf{I})$	Circularly symmetric complex Gaussian (CSCG)
$\mathbb{E}\{\cdot\}$	Expectation operation
$\mathrm{Tr}(\mathbf{D})$	Trace operation
$\lvert\mathbf{D}\rvert$	Determinant
$\lVert\mathbf{D}\rVert_{\mathrm{F}}$	Frobenius norm
$(\mathbf{D})^{\mathrm{T}}$	Transpose operator
$(\mathbf{D})^{\mathrm{H}}$	Hermitian operator
$(\mathbf{D})^{\star}$	Optimal value
$\mathrm{Re}\{.\}$	Real component of complex entry
$\lVert\mathbf{D}\rVert_2$	Second norm
$\mathbb{C}^{M\times N}$	space of $M \times N$ complex-valued matrices

II. System Model and Preliminaries

The considered system model is an FD scenario where a BS operates in FD mode with M_t transmit antennas and M_r receive antennas. Here, the BS simultaneously serves D DL and U UL single-antenna users as illustrated in Fig. 1. The channels from between BS to d-th DL user, u-th UL user to BS, u-th UL user to d-th DL user and SI channel are represented as $\mathbf{g}_d^{DL} \in \mathbb{C}^{M_t\times 1}, d \in \mathcal{D}$, $\mathbf{g}_u^{UL} \in \mathbb{C}^{M_r\times 1}, u \in \mathcal{U}$, $h_{u,d} \in \mathbb{C}, u \in \mathcal{U}, d \in \mathcal{D}$ and $\mathbf{F} \in \mathbb{C}^{M_t\times M_r}$ respectively. The list of symbols used in this paper is depicted in Table III.

In the considered FD-RSMA system, the BS transmits a set of original messages denoted as $\mathcal{M}^{DL} \triangleq \{M_1^{DL},\ldots,M_D^{DL}\}$

TABLE III: List of symbols used.

D	Number of DL users
U	Number of UL users
M_r	Number of receiving antennas at BS
M_t	Number of transmit antennas at BS
$\mathcal{J}$	$\{1,\ldots,J\}$
$\mathcal{D}$	$\{1,\ldots,D\}$
$\mathcal{U}$	$\{1,\ldots,U\}$
$\mathcal{R}$	$\{1,\ldots,M_r\}$
$\mathcal{T}$	$\{1,\ldots,M_t\}$
$\mathbf{g}_d^{DL} \in \mathbb{C}^{M_t\times 1}$	Channel between BS to d-th DL user
$\mathbf{g}_u^{UL} \in \mathbb{C}^{1\times M_r}$	Channel between u-th UL user to BS
$h_{d,u} \in \mathbb{C},$	Channel between u-th UL user to d-th DL user
$\mathbf{F} \in \mathbb{C}^{M_t\times M_r}$	SI channel
$\mathbf{w}_{\mathrm{c}} \in \mathbb{C}^{M_t\times 1}$	Transmit beamformer for the common stream
$\mathbf{w}_d \in \mathbb{C}^{M_t\times 1}$	Transmit beamformer for the private stream
$\mathbf{z}_u \in \mathbb{C}^{M_r\times 1}$	Receive beamformer for the u-th UL user

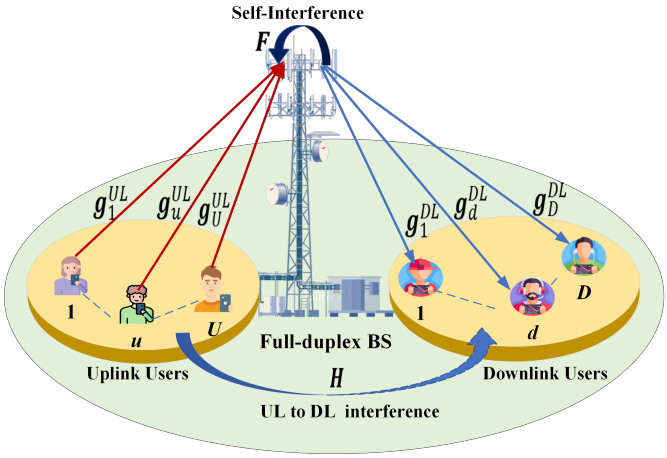

Fig. 1: System model.

to the DL users. For each d-th DL user, the message M_d^{DL} undergoes a division into two parts: the common message, denoted as $M_{d,\mathrm{c}}^{DL} \in \mathbb{C}$, and the private message, denoted as $M_{d,\mathrm{p}}^{DL} \in \mathbb{C}$. It is ensured that $\mathbb{E}[M_{d,\mathrm{c}}^{DL}(M_{d,\mathrm{c}}^{DL})^H] = 1$ and $\mathbb{E}[M_{d,\mathrm{p}}^{DL}(M_{d,\mathrm{p}}^{DL})^H] = 1$ for all $d \in \mathcal{D}$. Specifically, all DL user's common messages and the distinct dedicated private messages are encoded by the BS into a unified data stream s_{c}^{DL} and s_d^{DL} for each d-th DL user respectively. Consequently, the BS transmits a superimposed symbol given by

$$\mathbf{x}_T = \mathbf{w}_{\mathrm{c}} s_{\mathrm{c}}^{DL} + \sum_{d\in\mathcal{D}} \mathbf{w}_d s_k^{DL}, \tag{1}$$

where $\mathbf{w}_{\mathrm{c}} \in \mathbb{C}^{M_t\times 1}$ and $\mathbf{w}_d \in \mathbb{C}^{M_t\times 1}, \forall d \in \mathcal{D}$ are the transmit beamformers for the common stream and a private stream of d-th DL user, respectively.

Additionally, each UL user divides its original messages, denoted as W_u^{UL}, into two separate sub-messages. $W_{u,1}^{UL}$ and $W_{u,2}^{UL}$ such that $\mathbb{E}[W_{u,j}^{UL}(W_{u,j}^{UL})^H] = 1, \forall j \in \mathcal{J} \triangleq \{1\ldots J\}, \forall u \in \mathcal{U}$. These sub-messages are subsequently encoded into distinct streams $s_{u,j}^{UL}, \forall u, \forall j$ and are then transmitted to the BS from the UL users. Thus, the transmitted

signal by each u-th UL user is expressed as

$$x_u^{UL} = \sum_{j\in\mathcal{J}} \sqrt{p_{u,j}} s_{u,j}^{UL}, \forall\, u \in \mathcal{U}, \tag{2}$$

where $p_{u,j}, \forall\, u \in \mathcal{U},\ \forall\, j \in \mathcal{J}$ is the transmit power of the j-th message of u-th UL user. The signal received by the d-th DL user is expressed as

$$\begin{aligned} y_d =& (\mathbf{g}_d^{DL})^{\mathrm{H}} \mathbf{x}_T + \sum_{u\in\mathcal{U}} h_{d,u} x_u^{UL} + \eta_d \\ =& (\mathbf{g}_d^{DL})^{\mathrm{H}} \mathbf{w}_c s_c^{DL} + (\mathbf{g}_d^{DL})^{\mathrm{H}} \sum_{i\in\mathcal{D}} \mathbf{w}_i s_i^{DL} \\ &+ \underbrace{\sum_{u\in\mathcal{U}} \sum_{j\in\mathcal{J}} h_{d,u} \sqrt{p_{u,j}} s_{u,j}^{UL}}_{\text{UDI}} + \eta_d^{DL}, \end{aligned} \tag{3}$$

where $\eta_d^{DL} \sim \mathcal{CN}\left(0, (\sigma_d^{DL})^2\right)$ denotes the additive white Gaussian noise (AWGN) with zero mean and variance of $(\sigma_d^{DL})^2$ at the d-th DL user. The signal received by the d-th DL user comprises the desired signal from the BS, interference from UL users, referred to as UL to DL users interference (UDI), the interference from other DL users, termed as inter-user interference (IUI), and noise. Thus the received signal at the BS is expressed as

$$\boldsymbol{y}_B = \sum_{u\in\mathcal{U}} \mathbf{g}_u^{UL} x_u^{UL} + \mathbf{F}^{\mathrm{H}} \mathbf{x}_T + \boldsymbol{\eta}_B \tag{4}$$

$$\begin{aligned} =& \sum_{u\in\mathcal{U}} \mathbf{g}_u^{UL} \sum_{j\in\mathcal{J}} \sqrt{p_{u,j}} s_{u,j}^{UL} \\ &+ \underbrace{\mathbf{F}^{\mathrm{H}} \left(\mathbf{w}_c s_c^{DL} + \sum_{d\in\mathcal{D}} \mathbf{w}_d s_d^{DL} \right)}_{SI} + \boldsymbol{\eta}_B, \end{aligned} \tag{5}$$

where $\boldsymbol{\eta_B} \sim \mathcal{CN}\left(\mathbf{0}, (\sigma_{BS}^{UL})^2 I_{M_r}\right)$ at the BS. Therefore, the signal received at the BS is a combination of UL user messages, SI, and noise.

A. Achievable rate

In DL RSMA, each DL user decodes the common stream by considering all private streams as IUI along with UDI and noise. After the DL user uses SIC to decode the common stream, it's removed from the received signal. The resulting signal-to-interference-plus-noise ratio (SINR) for this stream at the d-th DL user can be written as

$$\gamma_{\mathrm{c},d}^{DL} = \frac{|(\mathbf{g}_d^{DL})^{\mathrm{H}} \mathbf{w}_{\mathrm{c}}|^2}{\sum_{i\in\mathcal{D}} |(\mathbf{g}_d^{DL})^{\mathrm{H}} \mathbf{w}_i|^2 + \sum_{u\in\mathcal{U}} \sum_{j\in\mathcal{J}} p_{u,j}^{UL} |h_{d,u}|^2 + (\sigma_{\mathrm{c},d}^{DL})^2}. \tag{6}$$

Using (6), the common rate is computed as

$$R_{\mathrm{c},d}^{DL} = \log_2(1 + \gamma_{\mathrm{c},d}^{DL}), \forall\, d \in \mathcal{D}. \tag{7}$$

To guarantee successful decoding of the common stream by all DL users, the common stream rate R_{c}^{DL} must be set as the minimum among the common rates of all users. This minimum-rate approach ensures that

$$R_{\mathrm{c}}^{DL} = \min\{R_{\mathrm{c},1}^{DL} \ldots R_{\mathrm{c},D}^{DL}\}. \tag{8}$$

Additionally, during d-th private stream decoding, other private streams contribute to the interference alongside undesirable interference (UDI) and noise. The SINR for the d-th private stream at the corresponding DL user is formulated as

$$\gamma_{\mathrm{p},d}^{DL} = \frac{|(\mathbf{g}_d^{DL})^{\mathrm{H}} \mathbf{w}_d|^2}{\sum_{i\in\mathcal{D}, i\neq d} |(\mathbf{g}_d^{DL})^{\mathrm{H}} \mathbf{w}_i|^2 + \sum_{u\in\mathcal{U}} \sum_{j\in\mathcal{J}} p_{u,j}^{UL} |h_{d,u}|^2 + (\sigma_d^{DL})^2}. \tag{9}$$

From (9), the private rate is expressed by

$$R_{\mathrm{p},d}^{DL} = \log_2(1 + \gamma_{\mathrm{p},d}^{DL}), \forall\, d \in \mathcal{D}. \tag{10}$$

The rate at the d-th DL user is computed by

$$R_{d,tot}^{DL} = C_d^{DL} + R_{\mathrm{p},d}^{DL}, \forall\, d \in \mathcal{D}, \tag{11}$$

where C_d^{DL} is part of the common rate intended for d-th DL user such that $\sum_d C_d^{DL} = R_c^{DL}$.

In the UL, the BS employs SIC to decode all sub-messages transmitted by UL users. The decoding order is predefined, where the initial sub-message of the order are decoded first, followed by the subsequent elements. At the BS, sub-messages with priorities lower than $s_{u,j}^{UL}$ are decoded and removed first, treating the rest as interference. This follows the approach in [46]. We use a specific decoding order called Π [46] to achieve fair treatment for all users such that

$$\begin{aligned} \Pi =& \{(s_{u,j}^{Ul} \to s_{u',j}^{Ul} \to s_{u,j'}^{Ul} \to s_{u',j'}^{Ul}) : \\ & \left|\mathbf{g}_u^{UL}\right| \geq \left|\mathbf{g}_{u'}^{UL}\right|, l \neq u', u, u' \in \mathcal{U}, j, j' \in \mathcal{J}\}. \end{aligned} \tag{12}$$

Although an efficient digital SI cancellation technique is assumed to be utilized, residual self-interference resulting from practical hardware limitations still remains despite assumptions that a digital SI cancellation technique is utilized [14]. Consequently, the SINR to decode $s_{u,j}^{Ul}$ sub-message of the u-th user can be expressed as

$$\gamma_{u,j}^{UL} = \frac{p_{u,j}^{UL} |(\mathbf{g}_u^{UL} \mathbf{z}_u|^2}{\sum_{(m,n)\in\mathcal{Q}_{u,j}} p_{m,n}^{UL} |\mathbf{g}_m^{UL} \mathbf{z}_m|^2 + \left(P_{SI} + \sigma_{BS}^{UL^2}\right)}, \tag{13}$$

where $\mathbf{z}_u \in \mathbb{C}^{M_r \times 1}$ denotes the receive beamformer at the BS to decode the signal from the u-th UL user, $\mathcal{Q}_{u,j}$ represents the set of all the messages which have higher decoding order than $s_{u,j}^{UL}$ and $P_{SI} = \omega(|\mathbf{F}^{\mathrm{H}} \mathbf{w}_{\mathrm{c}}|^2 + \sum_{d\in\mathcal{D}} |\mathbf{F}^{\mathrm{H}} \mathbf{w}_k|^2)$ such that ω is the RSI coefficient. Thus, the overall rate for the u-th user can be obtained as

$$R_u^{UL} = \sum_{j\in\mathcal{J}} R_{u,j}^{UL} = \sum_{j\in\mathcal{J}} \log_2(1 + \gamma_{u,j}^{UL}), \forall\, u \in \mathcal{U}. \tag{14}$$

The SE for the considered system is expressed as

$$SE = \sum_{d\in\mathcal{D}} (C_d^{DL} + R_{\mathrm{p},d}^{DL}) + \sum_{u\in\mathcal{U}} R_u^{UL}. \tag{15}$$

B. Power consumption model and Energy Efficiency

The total power consumption of the FD-RSMA system depends on the transmit power at the BS and the UL users and the constant power consumed by the circuitry denoted as P_C. The total power consumption of the system is given by

$$P_T = \left(\sum_{d \in \mathcal{D}} |\mathbf{w}_d, |^2 + |\mathbf{w}_c|^2 \right) + \sum_{u \in \mathcal{U}} \sum_{j \in \mathcal{J}} p_{u,j}^{UL} + P_C, \quad (16)$$

Apparently, the EE of the considered system is given by

$$EE = \frac{SE}{P_T}. \quad (17)$$

C. Channel state information

In communications systems, the BS must be capable of determining the SINRs at the receivers based on the precoder. However, this process demands accurate information about the channels to the receivers, known as CSI. In frequency division duplexing (FDD) systems, the BS acquires the necessary CSI by sending training symbols to users. Each user then estimates the channel coefficients and sends a quantized version of the estimated channel vector back to the BS. Thus, BS only has estimates of the CSI, leading to uncertainty in SINR estimation for each receiver. Consequently, the precoder design needs to be carried out in the presence of this uncertainty in the estimates.

In practice, due to several unwanted obstacles such as hardware impairments, fading in the channel, etc., CSI may suffer an estimation error. For example, the CSI from the BS to the d-th DL user, from the u-th UL user to the BS, and the UDI channel from u-th UL user to d-th DL user can be expressed as $\mathbf{g}_d^{DL} = \tilde{\mathbf{g}}_d^{DL} + \Delta\mathbf{g}_d^{DL}$, $\mathbf{g}_u^{UL} = \tilde{\mathbf{g}}_u^{UL} + \Delta\mathbf{g}_u^{UL}$, and $h_{d,u} = \tilde{h}_{d,u} + \Delta h_{d,u}$ respectively, where $\tilde{\mathbf{g}}_d^{DL}$, $\tilde{\mathbf{g}}_u^{UL}$, and $\tilde{h}_{d,u}$ denotes estimated CSI and $\Delta\mathbf{g}_d^{DL}$, $\Delta\mathbf{g}_u^{UL}$, and $\Delta h_{d,u}$ indicates error matrices. In this work, these imperfections are modeled using the norm-bounded error model [47] given by

$$\left\|\Delta\mathbf{g}_d^{DL}\right\|_2 \leq \varrho_d;\ \left\|\Delta\mathbf{g}_u^{UL}\right\|_2 \leq \varepsilon_u;\ |\Delta h_{d,u}| \leq \varpi_{d,u}, \quad (18)$$

where ϱ_d, ε_u and $\varpi_{d,u}$ denote the DL,UL, and UDI channel's error bound respectively. Considering these uncertainties, the DL,UL, and UDI imperfect channels lie in the bounded region ($\mathcal{B}$), ($\mathcal{F}$). and ($\mathcal{G}$) defined as

$$\mathbf{g}_d^{DL} \in \mathcal{B} = \left\{ \tilde{\mathbf{g}}_d^{DL} + \Delta\mathbf{g}_d^{DL} : \left\|\Delta\mathbf{g}_d^{DL}\right\|_2 \leq \varrho_d \right\}, \quad (19)$$

$$\mathbf{g}_u^{UL} \in \mathcal{F} = \left\{ \tilde{\mathbf{g}}_u^{UL} + \Delta\mathbf{g}_u^{UL} : \left\|\Delta\mathbf{g}_u^{UL}\right\|_2 \leq \varepsilon_u \right\}, \quad (20)$$

$$h_{d,u} \in \mathcal{G} = \left\{ \tilde{h}_{d,u} + \Delta h_{d,u} : |\Delta h_{d,u}| \leq \varpi_{d,u} \right\}. \quad (21)$$

III. Problem formulation

Notably, the SE increases as the power consumption for transmission increases. To maximize the SE, it is necessary to use all available transmit power. However, this approach may not be ideal for maximizing EE, as EE aims to achieve a balance between SE and power consumption. As a result, SE and EE are in conflict in the moderate and high signal-to-noise ratio (SNR) regimes, leading to a trade-off between the two metrics. In this subsection, we explore this trade-off and determine the optimal resource allocation design strategy that strikes the best balance between SE and EE. We denote $\mathbf{\Upsilon}_T = \{\mathbf{g}_d^{DL} \in \mathcal{B},\ \mathbf{g}_u^{UL} \in \mathcal{F},\ h_{d,u} \in \mathcal{G}, \forall d \in \mathcal{D}, u \in \mathcal{U}\}$ and $\mathbf{\Upsilon}_d = \{\mathbf{g}_d^{DL} \in \mathcal{B},\ h_{d,u} \in \mathcal{G}, \forall d \in \mathcal{D}, u \in \mathcal{U}\}$. The SE-EE trade-off can be viewed as a MOO problem given by

$$(P1): \max_{\mathbf{w}_c, \mathbf{w}, \mathbf{z}, \mathbf{P}, \mathbf{c}} \min_{\mathbf{\Upsilon}} SE(\mathbf{w}_c, \mathbf{w}, \mathbf{z}, \mathbf{P}, \mathbf{c}) \quad (22a)$$

$$\max_{\mathbf{w}_c, \mathbf{w}, \mathbf{z}, \mathbf{P}, \mathbf{c}} \min_{\mathbf{\Upsilon}} EE(\mathbf{w}_c, \mathbf{w}, \mathbf{z}, \mathbf{P}, \mathbf{c}) \quad (22b)$$

$$\text{s.t. } (C.1): \sum_{d \in \mathcal{D}} |\mathbf{w}_d|^2 + |\mathbf{w}_c|^2 \leq p_{max}^{DL}, \quad (22c)$$

$$(C.2): \sum_{i \in \mathcal{D}} C_i^{DL} \leq R_{c,d}^{DL}, \forall\, \mathbf{\Upsilon}_d, \forall d \in \mathcal{D} \quad (22d)$$

$$(C.3): C_d^{DL} \geq 0, \forall d \in \mathcal{D} \quad (22e)$$

$$(C.4): R_{d,tot}^{DL} \geq R_{d,min}^{DL}, \forall\, \mathbf{\Upsilon}_d, \forall d \in \mathcal{D} \quad (22f)$$

$$(C.5): \sum_{j \in \mathcal{J}} p_{u,j}^{UL} \leq p_{u,max}^{UL}, \forall u \in \mathcal{U}, \quad (22g)$$

$$(C.6): \sum_{j \in \mathcal{J}} R_{u,j}^{UL} \geq R_{u,min}^{UL}, \forall \mathbf{g}_u^{UL} \in \mathcal{F}, u \in \mathcal{U}, \quad (22h)$$

$$(C.7): |\mathbf{z}_m| = 1, \forall m \in \mathcal{U}. \quad (22i)$$

where $\mathbf{w} = \{\mathbf{w}_1, \ldots, \mathbf{w}_D\}$, $\mathbf{z} = \{\mathbf{z}_1, \ldots, \mathbf{z}_U\}$, $\mathbf{P} = \{p_{1,1}^{UL}, \ldots, p_{U,J}^{UL}\}$ and $\mathbf{c} = \{C_1^{DL}, \ldots, C_D^{DL}\}$. $(C.1)$ and $(C.5)$ are the constraints to limit the transmit power at the BS and at each UL user, and to ensure that they don't exceed p_{max}^{DL} and $p_{u,max}^{UL}$, respectively. Constraints $(C.2)$ and $(C.3)$ guarantee successful decoding of the common stream by all DL users. Additionally, a minimum quality of service (QoS) for each DL and UL user is guaranteed by the constraints $(C.4)$ and $(C.6)$, where $R_{d,min}^{DL}$ and $R_{u,min}^{UL}$ denote the minimum acceptable data rates. Finally, constraint $(C.7)$ specifies the unit power of the receiving beamformer.

In particular, the resource allocation problem in (22) is an NP-hard non-convex optimization problem that is generally intractable. Specifically, we epitomize the prime challenges in solving (22) as follows:

1) The optimization problem stated in (22) poses challenges due to its non-convex multi-objective functions and constraints. Additionally, the rate expression has a complex relationship with optimization variables, making it difficult to find a solution.
2) The joint optimization of transmit and receive beamforming variables, further complicates the problem and increases its computational complexity.
3) Currently, exhaustive search can provide globally optimal solutions for these non-convex problems within a polynomial time frame.
4) While an exhaustive search can theoretically find the optimal solution, the exponential growth of computational complexity with the total number of variables makes it impractical to implement in practice.

Given the inherent difficulties in finding an optimal solution to the optimization problem given in (22), a practical approach

is to seek a high-quality sub-optimal solution for the resource allocation problem. In the following section, we address the challenges mentioned above and propose an efficient and effective resource allocation scheme. The objective is to develop a solution that strikes a balance between computational complexity and performance, providing significant improvements over existing approaches.

A. Proposed solution

To handle the conflicting objectives in problem (P1), we use the weighted sum method, which converts the MOO problem to the SOO problem by prioritizing each objective function. The RE objective function of the SOO problem is given by

$$\mathcal{O}_{_{EE-SE,1}} = \frac{\varrho}{\varphi_{EE}} EE + \frac{(1-\varrho)}{\varphi_{SE}} SE, \tag{23}$$

where ϱ is the trade-off parameter and φ_{EE} and φ_{SE} are the normalization factors. Due to the fractional form of the objective function in (23), solving it directly is challenging. To address this, we apply the Dinkelbach method [41], which converts the fractional form into a subtractive form. Consequently, the objective function in (23) is transformed as

$$\mathcal{O}_{_{EE-SE,2}} = \varphi_{_{SE-EE}} SE - qP_T, \tag{24}$$

where $\varphi_{_{SE-EE}} = (\varrho\varphi_{SE} + (1-\varrho)\varphi_{EE})/(\varphi_{SE}\varphi_{EE})$ and q is the network price. By dividing the transformed objective function with $\varphi_{_{SE-EE}}$, (24) is transformed as

$$\mathcal{O}_{_{EE-SE,3}} = SE - \left(\frac{qP_T}{(\varphi_{_{SE-EE}})}\right). \tag{25}$$

By replacing the positive constant $q/\varphi_{_{SE-EE}}$ with $\chi/(1-\chi)$, for $0 < \chi < \chi_{EE} < 1$, where $\chi_{EE}/(1-\chi_{EE}) = q\varphi_{EE}/\varphi_{SE}$ and multiplying with $(1-\chi)$, (25) is written as

$$\mathcal{O}_{_{EE-SE,4}} = (1-\chi)SE - \chi P_T. \tag{26}$$

The objective function $\mathcal{O}_{_{EE-SE,4}}$ in equation (26) transforms the SE-EE trade-off problem, with ϱ as the trade-off parameter, into a SE-PT trade-off problem with χ as the trade-off parameter. $\mathcal{O}_{_{EE-SE,4}}$ seeks to maximize SE while minimizing total power consumption. Consequently, the solution to the MOO problem in (P1) can be derived from the subsequent SOO problem, as follows:

$$(P2)\colon \max_{\mathbf{w}_c,\mathbf{w},\mathbf{z},\mathbf{P},\mathbf{c}} \min_{\boldsymbol{\Upsilon}} \frac{(1-\chi)}{\xi_{SE}} SE - \frac{\chi}{\xi_{PT}} P_T \tag{27a}$$

$$\text{s.t. } (C.1), \ldots, (C.6), \tag{27b}$$

where ξ_{SE} and ξ_{PT} are the normalizing factors, calculated by maximizing SE and minimizing P_T respectively [33]. At $\chi = 0$, the problem (P2) can be simplified to maximize SE, while at $\chi = 1$, the problem reduces to minimizing power consumption. The energy-efficient solution is achieved at χ_{EE}.

The formulated in problem (P2) is non-convex due to the coupling of variables in the objective functions (27a), constraints $(C.2)$, $(C.4)$ and $(C.6)$. Given the non-convexity of the optimization problems within (P2), achieving globally optimal solutions in polynomial time through standard mathematical optimization methods remains intractable. Consequently, pursuing high-quality sub-optimal solutions for the resource allocation tasks becomes a more attractive approach. In pursuit of tractability, we employ a matched-filter design principle for the m^{th} receive beamformer at the BS, drawing inspiration from [48]. This criterion dictates that $\mathbf{z}_{_m} = \mathbf{g}_m^{UL}/||\mathbf{g}_m^{UL}||$. We utilize successive convex approximation and SDP to design the optimization variables [49]. Necessary for our later derivations, two useful lemmas concerning multiple complex values uncertainties are introduced as follows.

Lemma 1. *(General S-Procedure) Define the quadratic functions of the variable $\mathbf{x} \in \mathbb{C}^{n\times 1}$:*

$$p_i(\mathbf{x}) = \mathbf{x}^H \mathbf{U}_i \mathbf{x} + 2\mathrm{Re}\{\mathbf{u}_i^H \mathbf{x}\} + u_i, i = 0, \cdots, T,$$

where $\mathbf{U}_i = \mathbf{U}_i^H$. The condition $\{p_i(\mathbf{x}) \geq 0\}_{i=1}^T \Rightarrow p_0(\mathbf{x}) \geq 0$ is satisfied if only there exist $\forall i, \varpi_i \geq 0$ such that

$$\begin{bmatrix} \mathbf{U}_0 & \mathbf{u}_0 \\ \mathbf{u}_0^H & u_0 \end{bmatrix} - \sum_{i=1}^{T} \varpi_i \begin{bmatrix} \mathbf{U}_i & \mathbf{u}_i \\ \mathbf{u}_i^H & u_i \end{bmatrix} \succeq 0.$$

Lemma 2. *(General sign-definiteness) For a given set of matrix $\mathbf{U} = \mathbf{U}^H$, $\{\mathbf{Y}_i, \mathbf{Z}_i\}_{i=1}^T$, the following LMI satisfies*

$$\mathbf{U} \succeq \sum_{i=1}^{T} \left(\mathbf{Y}_i^{\mathrm{H}} \mathbf{X}_i \mathbf{Z}_i + \mathbf{Z}_i^{\mathrm{H}} \mathbf{X}_i^{\mathrm{H}} \mathbf{Y}_i\right), \forall i, ||\mathbf{X}_i||_F \leq \rho_i,$$

if and only if there exist real numbers $\forall i$, $\mu_i \geq 0$ such that

$$\begin{bmatrix} \mathbf{U} - \sum\limits_{i=1}^{T} \mu_i \mathbf{Z}_i^{\mathrm{H}} \mathbf{Z}_i & -\rho_1 \mathbf{Y}_1^{\mathrm{H}} & \cdots & -\rho_T \mathbf{Y}_T^{\mathrm{H}} \\ -\rho_1 \mathbf{Y}_1 & \mu_1 \mathbf{I} & \cdots & \mathbf{0} \\ \vdots & \vdots & \ddots & \vdots \\ -\rho_T \mathbf{Y}_T & \mathbf{0} & \cdots & \mu_T \mathbf{I} \end{bmatrix} \succeq \mathbf{0}.$$

It is noted that **Lemma 2** can be proved by applying **Lemma 1** and the detailed proof is given in [50].

The problem to optimize $\mathbf{w}_{_c}, \mathbf{w}, \mathbf{P}, \mathbf{c}$ (i.e. problem (P2)) can be reformulated as

$$(P3)\colon \max_{\mathbf{w}_c,\mathbf{w},\mathbf{P},\mathbf{c}} \min_{\boldsymbol{\Upsilon}} \frac{(1-\chi)}{\xi_{SE}} SE - \frac{\chi}{\xi_{PT}} P_T \tag{28a}$$

$$\text{s.t. } (C.1), \ldots, (C.6). \tag{28b}$$

Using auxiliary variables $\lambda_{\mathrm{c},d}^{DL}$, $\lambda_{\mathrm{p},d}^{DL}$, $\lambda_{u,j}^{UL}$, $\mu_{\mathrm{c},d}^{DL}$, $\mu_{\mathrm{p},d}^{DL}$ and $\mu_{u,j}^{UL}$ the expressions in (6), (9) and (13) are relaxed as follows

$$|(\mathbf{g}_d^{DL})^{\mathrm{H}} \mathbf{w}_{_c}|^2 \leq \lambda_{\mathrm{c},d}^{DL} \mu_{\mathrm{c},d}^{DL}, \forall \mathbf{g}_d^{DL} \in \mathcal{B}, d \in \mathcal{D}, \tag{29}$$

$$|(\mathbf{g}_d^{DL})^{\mathrm{H}} \mathbf{w}_{_d}|^2 \leq \lambda_{\mathrm{p},d}^{DL} \mu_{\mathrm{p},d}^{DL}, \forall \mathbf{g}_d^{DL} \in \mathcal{B}, d \in \mathcal{D}, \tag{30}$$

$$|\mathbf{g}_u^{UL} \mathbf{z}_{_u}|^2 \leq \lambda_{u,j}^{UL} \mu_{u,j}^{UL} / p_{_{u,j}}^{UL}, \forall \mathbf{g}_u^{UL} \in \mathcal{F}, u \in \mathcal{U}, j \in \mathcal{J}, \tag{31}$$

where

$$\mu_{\mathrm{c},d}^{DL} \geq \sum_{i\in\mathcal{D}} |(\mathbf{g}_d^{DL})^{\mathrm{H}} \mathbf{w}_{_i}|^2 + \sum_{u\in\mathcal{U}} \sum_{j\in\mathcal{J}} p_{_{u,j}}^{UL} |h_{_{d,u}}|^2 + (\sigma_{\mathrm{c},d}^{DL})^2, \tag{32}$$

$$\mu_{\mathrm{p},d}^{DL} \geq \sum_{\substack{i\in\mathcal{D}, \\ i\neq d}} |(\mathbf{g}_d^{DL})^{\mathrm{H}} \mathbf{w}_{_i}|^2 + \sum_{u\in\mathcal{U}} \sum_{j\in\mathcal{J}} p_{_{u,j}}^{UL} |h_{_{d,u}}|^2 + (\sigma_d^{DL})^2, \tag{33}$$

$$\mu_{u,j}^{UL} \geq \sum_{(m,n)\in\mathcal{Q}_{u,j}} p_{_{m,n}}^{UL} |\mathbf{g}_m^{UL} \mathbf{z}_{_m}|^2 + P_{SI} + {\sigma_{BS}^{UL}}^2. \tag{34}$$

Lemma 3 is introduced to approximate the constraint (29) at $\mathbf{w}_{\mathrm{c}}^{(i)}$.

Lemma 3. *At* $\mathbf{w}_{c}^{(i)}$*, substituting* $\mathbf{g}_d^{DL} = \tilde{\mathbf{g}}_d^{DL} + \Delta\mathbf{g}_d^{DL}$*, the lower bound of the left side of constraint* (29) *can be approximated as*

$$(\Delta\mathbf{g}_d^{DL})^{\mathrm{H}}\mathbf{A}_{c,d}\Delta\mathbf{g}_d^{DL}+2Re\{\mathbf{a}_{c,d}^{\mathrm{H}}\Delta\mathbf{g}_d^{DL}\}+a_{c,d}, \tag{35}$$

where $\mathbf{A}_{c,d} = 2Re\{\mathbf{w}_{\mathrm{c}}(\mathbf{w}_{c}^{(i)})^{\mathrm{H}}\} - \mathbf{w}_{c}^{(i)}(\mathbf{w}_{\mathrm{c}}^{(i)})^{\mathrm{H}}$*,* $\mathbf{a}_{c,d} = (\mathbf{A}_{c,d})^{\mathrm{H}}\tilde{\mathbf{g}}_d^{DL}$*,* $a_{c,d} = (\tilde{\mathbf{g}}_d^{DL})^{\mathrm{H}}\mathbf{A}_{c,d}\tilde{\mathbf{g}}_d^{DL}$.

Proof. Firstly, $|(\mathbf{g}_d^{DL})^{\mathrm{H}}\mathbf{w}_{\mathrm{c}}|^2$ is approximated at $\mathbf{w}_{\mathrm{c}}^{(i)}$ using a first-order Taylor expansion, thus the inequality with lower bound is written as

$$\begin{aligned}|(\mathbf{g}_d^{DL})^{\mathrm{H}}\mathbf{w}_{\mathrm{c}}|^2 \leq\ & 2Re\{(\mathbf{g}_d^{DL})^{\mathrm{H}}\mathbf{w}_{\mathrm{c}}^{(i)}\mathbf{w}_{\mathrm{c}}^{\mathrm{H}}\mathbf{g}_d^{DL}\}\\ & - (\mathbf{g}_d^{DL})^{\mathrm{H}}\mathbf{w}_{\mathrm{c}}^{(i)}\mathbf{w}_{\mathrm{c}}^{(i),\mathrm{H}}\mathbf{g}_d^{DL}.\end{aligned} \tag{36}$$

Replacing $\mathbf{g}_d^{DL}$ with $\tilde{\mathbf{g}}_d^{DL}+\Delta\mathbf{g}_d^{DL}$ in (36), (36) is expressed as (37) given in the top of the next page. $|(\mathbf{g}_d^{DL})^{\mathrm{H}}\mathbf{w}_{\mathrm{c}}|^2$ can be expressed as $(\Delta\mathbf{g}_d^{DL})^{\mathrm{H}}\mathbf{A}_{\mathrm{c},d}\Delta\mathbf{g}_d^{DL}+2Re\{\mathbf{a}_{\mathrm{c},d}^{\mathrm{H}}\Delta\mathbf{g}_d^{DL}\}+a_{\mathrm{c},d}$, which completes the proof. □

Using **Lemma 3**, constraint (29) is approximated as

$$(\Delta\mathbf{g}_d^{DL})^{\mathrm{H}}\mathbf{A}_{\mathrm{c},d}\Delta\mathbf{g}_d^{DL}+2Re\{\mathbf{a}_{\mathrm{c},d}^{\mathrm{H}}\Delta\mathbf{g}_d^{DL}\}+a_{\mathrm{c},d} \leq \tilde{\lambda}_{\mathrm{c},d}^{DL}, \tag{38}$$

where $\tilde{\lambda}_{\mathrm{c},d}^{DL} = \lambda_{\mathrm{c},d}^{DL}(\mu_{\mathrm{c},d}^{DL})^{(i)} + (\lambda_{\mathrm{c},d}^{DL})^{(i)}\mu_{\mathrm{c},d}^{DL} - (\lambda_{\mathrm{c},d}^{DL})^{(i)}(\mu_{\mathrm{c},d}^{DL})^{(i)}$.

Similarly, the inequality (30) is linearly approximated at $\mathbf{w}_{d}^{(i)}$, $p_{u,j}^{UL(i)}$, $\mu_{\mathrm{c},d}^{DL(i)}$, $\mu_{\mathrm{p},d}^{DL(i)}$ and $\mu_{u,j}^{UL(i)}$ are given as

$$(\Delta\mathbf{g}_d^{DL})^{\mathrm{H}}\mathbf{A}_{\mathrm{p},d}\Delta\mathbf{g}_d^{DL}+2Re\{\mathbf{a}_{\mathrm{p},d}^{\mathrm{H}}\Delta\mathbf{g}_d^{DL}\}+a_{\mathrm{p},d} \leq \tilde{\lambda}_{\mathrm{p},d}^{DL}, \tag{39}$$

where

$$\tilde{\lambda}_{\mathrm{p},d}^{DL} = \lambda_{\mathrm{p},d}^{DL}(\mu_{\mathrm{p},d}^{DL})^{(i)} + (\lambda_{\mathrm{p},d}^{DL})^{(i)}\mu_{\mathrm{p},d}^{DL} - (\lambda_{\mathrm{p},d}^{DL})^{(i)}(\mu_{\mathrm{p},d}^{DL})^{(i)},$$

$$\mathbf{A}_{\mathrm{p},d} = 2Re\{\mathbf{w}_{d}(\mathbf{w}_{d}^{(i)})^{\mathrm{H}}\} - \mathbf{w}_{d}^{(i)}(\mathbf{w}_{d}^{(i)})^{\mathrm{H}},$$
$$\mathbf{a}_{\mathrm{p},d} = (\mathbf{A}_{\mathrm{p},d})^{\mathrm{H}}\tilde{\mathbf{g}}_d^{DL}, a_{\mathrm{p},d} = (\tilde{\mathbf{g}}_d^{DL})^{\mathrm{H}}\mathbf{A}_{\mathrm{p},d}\tilde{\mathbf{g}}_d^{DL},$$

To handle the associated constraint in equation (38), the parameters in **Lemma 1** can be set as follows

$T = 1, \mathbf{U}_0 = \mathbf{A}_{\mathrm{c},d}, \mathbf{u}_0 = \mathbf{a}_{\mathrm{c},d}, u_0 = a_{\mathrm{c},d} - \tilde{\lambda}_{\mathrm{c},d}^{DL}, \mathbf{x} = \Delta\mathbf{g}_d^{DL}, \mathbf{U}_1 = -\mathbf{I}, u_1 = \phi_{\mathrm{c},d}^2$.

Using **Lemma 1**, the linear matrix inequality (LMI) of (38) is given as

$$\begin{bmatrix}\varkappa_{\mathrm{c},d}\mathbf{I}_{M_t} + \mathbf{A}_{\mathrm{c},d} & \mathbf{a}_{\mathrm{c},d}\\ \mathbf{a}_{\mathrm{c},d}^{\mathrm{H}} & c_{\mathrm{c},d}\end{bmatrix} \succeq \mathbf{0}, \forall d \in \mathcal{D}, \tag{40}$$

where $\varkappa_{\mathrm{c}} = \{\varkappa_{\mathrm{c},1} \ldots \varkappa_{\mathrm{c},D}\}$ are the slack variables and $c_{\mathrm{c},d} = a_{\mathrm{c},d} - \tilde{\lambda}_{\mathrm{c},d}^{DL} - \varkappa_{\mathrm{c},d}\phi_{\mathrm{c},d}$. Similarly, the LMI of the inequality in (39) is written as

$$\begin{bmatrix}\varkappa_{\mathrm{p},d}\mathbf{I}_{M_t} + \mathbf{A}_{\mathrm{p},d} & \mathbf{a}_{\mathrm{p},d}\\ \mathbf{a}_{\mathrm{p},d}^{\mathrm{H}} & c_{\mathrm{p},d}\end{bmatrix} \succeq \mathbf{0}, \forall d \in \mathcal{D}, \tag{41}$$

where $\varkappa_{\mathrm{p}} = \{\varkappa_{\mathrm{p},1} \ldots \varkappa_{\mathrm{p},D}\}$ are the slack variables and $c_{\mathrm{p},d} = a_{\mathrm{p},d} - \tilde{\lambda}_{\mathrm{p},d}^{DL} - \varkappa_{\mathrm{p},d}\phi_{\mathrm{p},d}$.

Note that constraints (40) and (41) are LMI's, which can be solved by convex optimization tools. Further, denoting $\mathbf{W} = [\mathbf{w}_1, \ldots, \mathbf{w}_D]$ and $\mathbf{W}_{-d} = [\mathbf{w}_1, \ldots, \mathbf{w}_{d-1}, \mathbf{w}_{d+1}, \ldots, \mathbf{w}_D]$ and using the triangle inequality property [31] i.e, $|x+y|^2 \leq (|x|+|y|)^2 = |x|^2+|y|^2+2|x|.|y|$, the semi-infinite inequality constraint in (32) and (33) are written as

$$||(\mathbf{g}_d^{DL})^{\mathrm{H}}\mathbf{W}||_2^2 \leq \mu_{\mathrm{c},d}^{DL} - \sum_{u\in\mathcal{U}}\sum_{j\in\mathcal{J}} p_{u,j}^{UL}\hat{h}_{d,u} - (\sigma_{\mathrm{c},d}^{DL})^2, \tag{42}$$

$$||(\mathbf{g}_d^{DL})^{\mathrm{H}}\mathbf{W}_{-d}||_2^2 \leq \mu_{\mathrm{p},d}^{DL} - \sum_{u\in\mathcal{U}}\sum_{j\in\mathcal{J}} p_{u,j}^{UL}\hat{h}_{d,u} - (\sigma_{d}^{DL})^2, \tag{43}$$

where $\hat{h}_{d,u}$ is given as

$$\begin{aligned}\hat{h}_{d,u} &\triangleq \max_{|\Delta h_{d,u}|\leq\varpi_{d,u}} |h_{d,u}|^2 = |\tilde{h}_{d,u} + \Delta h_{d,u}|^2\\ &\leq |\tilde{h}_{d,u}|^2 + \varpi_{d,u}^2 + 2|\tilde{h}_{d,u}|\varpi_{d,u}.\end{aligned} \tag{44}$$

Similarly, by adopting the Schur's complement [51], the LMI of (42) is written as

$$\begin{bmatrix}\tilde{\mu}_{\mathrm{c},d}^{DL} & \mathbf{b}_{\mathrm{c},d}^{H}\\ \mathbf{b}_{\mathrm{c},d} & \mathbf{I}\end{bmatrix} \succeq \mathbf{0}, \forall d \in \mathcal{D}, \tag{45}$$

where $\mathbf{b}_{\mathrm{c},d} = ((\mathbf{g}_d^{DL})^{\mathrm{H}}\mathbf{W})^H$ and $\tilde{\mu}_{\mathrm{c},d}^{DL} = \mu_{\mathrm{c},d}^{DL} - \sum_{u\in\mathcal{U}}\sum_{j\in\mathcal{J}} p_{u,j}^{UL}\hat{h}_{d,u} - (\sigma_{\mathrm{c},d}^{DL})^2$. To incorporate imperfect channels, $\mathbf{g}_{\mathrm{c},d}^{DL} = \tilde{\mathbf{g}}_{\mathrm{c},d}^{DL} + \Delta\mathbf{g}_{\mathrm{c},d}^{DL}$ is substituted in (45) and represented as follows

$$\begin{aligned}\begin{bmatrix}\tilde{\mu}_{\mathrm{c},d}^{DL} & \tilde{\mathbf{b}}_{\mathrm{c},d}^{H}\\ \tilde{\mathbf{b}}_{\mathrm{c},d} & \mathbf{I}\end{bmatrix} \succeq & -\begin{bmatrix}\mathbf{0}\\ \mathbf{W}^H\end{bmatrix}(\Delta\mathbf{g}_{\mathrm{c},d}^{DL})^{\mathrm{H}}\begin{bmatrix}\boldsymbol{I} & \mathbf{0}\end{bmatrix}\\ & -\begin{bmatrix}\boldsymbol{I}\\ \mathbf{0}\end{bmatrix}\Delta\mathbf{g}_{\mathrm{c},d}^{DL}\begin{bmatrix}\mathbf{0} & \mathbf{W}\end{bmatrix}, \forall d \in \mathcal{D},\end{aligned} \tag{46}$$

where $\tilde{\mathbf{b}}_{\mathrm{c},d} = ((\tilde{\mathbf{g}}_d^{DL})^{\mathrm{H}}\mathbf{W})^H$. To utilize **Lemma 2**, we introduce the following parameters for (46) as

$$\mathbf{U} = \begin{bmatrix}\tilde{\mu}_{\mathrm{c},d}^{DL} & \tilde{\mathbf{b}}_{\mathrm{c},d}^{H}\\ \tilde{\mathbf{b}}_{\mathrm{c},d} & \mathbf{I}\end{bmatrix}, \mathbf{Y}_1 = -\begin{bmatrix}\mathbf{0} & \mathbf{W}\end{bmatrix},$$
$$\mathbf{Z}_1 = \begin{bmatrix}\boldsymbol{I} & \mathbf{0}\end{bmatrix}, \mathbf{X}_1 = (\Delta\mathbf{g}_d^{DL})^{\mathrm{H}}.$$

Further, considering the worst-case scenario, the LMI of constraint (42) is given by

$$\begin{bmatrix}\tilde{\mu}_{\mathrm{c},d}^{DL} - \beta_{\mathrm{c},d} & \tilde{\mathbf{b}}_{\mathrm{c},d}^{H} & \mathbf{0}_{1\times M_t}\\ \tilde{\mathbf{b}}_{\mathrm{c},d} & \mathbf{I}_D & \varrho_d\mathbf{W}^H\\ \mathbf{0}_{M_t\times 1} & \varrho_d\mathbf{W} & \beta_{\mathrm{c},d}\mathbf{I}_{M_t}\end{bmatrix} \succeq \mathbf{0}, \forall d \in \mathcal{D}, \tag{47}$$

where $\boldsymbol{\beta}_{\mathrm{c}} = [\beta_{\mathrm{c},1}, \cdots, \beta_{\mathrm{c},D}]^{\mathrm{T}}$ represents the slack variables. Similarly the LMI for the constraint in (43) is written as

$$\begin{bmatrix}\tilde{\mu}_{\mathrm{p},d}^{DL} - \beta_{\mathrm{p},d} & \tilde{\mathbf{b}}_{\mathrm{p},d}^{H} & \mathbf{0}_{1\times M_t}\\ \hat{\mathbf{b}}_{\mathrm{p},d} & \mathbf{I}_{D-1} & \varrho_d\mathbf{W}_{-d}^H\\ \mathbf{0}_{M_t\times 1} & \varrho_d\mathbf{W}_{-d} & \beta_{\mathrm{p},d}\mathbf{I}_{M_t}\end{bmatrix} \succeq \mathbf{0}, \forall d \in \mathcal{D}, \tag{48}$$

where $\tilde{\mathbf{b}}_{\mathrm{p},d} = ((\tilde{\mathbf{g}}_d^{DL})^{\mathrm{H}}\mathbf{W}_{-d})^{\mathrm{H}}$ and $\tilde{\mu}_{\mathrm{p},d}^{DL} = \mu_{\mathrm{c},d}^{DL} - \sum_{u\in\mathcal{U}}\sum_{j\in\mathcal{J}} p_{u,j}^{UL}\hat{h}_{d,u} - (\sigma_{\mathrm{p},d}^{DL})^2$. $\boldsymbol{\beta}_{\mathrm{p}} = [\beta_{\mathrm{p},1}, \cdots, \beta_{\mathrm{p},D}]^{\mathrm{T}}$ represents the slack variables.

To tackle the semi-infinite inequality constraint in (34), we rewrite $|\mathbf{g}_m^{UL}\mathbf{z}_m|^2$ as

$$\begin{aligned}|\mathbf{g}_m^{UL}\mathbf{z}_m|^2 &= (\mathbf{z}_m)^{\mathrm{H}}((\tilde{\mathbf{g}}_m^{UL})^{\mathrm{H}}\tilde{\mathbf{g}}_m^{UL} + (\tilde{\mathbf{g}}_m^{UL})^{\mathrm{H}}\Delta\mathbf{g}_m^{UL} +\\ &\quad (\Delta\mathbf{g}_m^{UL})^{\mathrm{H}}\tilde{\mathbf{g}}_m^{UL} + (\Delta\mathbf{g}_m^{UL})^{\mathrm{H}}\Delta\mathbf{g}_m^{UL})\mathbf{z}_m,\\ &= \mathbf{z}_m^{\mathrm{H}}\left((\tilde{\mathbf{g}}_m^{UL})^{\mathrm{H}}\tilde{\mathbf{g}}_m^{UL} + \Lambda_m\right)\mathbf{z}_m.\end{aligned} \tag{49}$$

$$(\tilde{\mathbf{g}}_d^{DL}+(\Delta\mathbf{g}_d^{DL})^{\mathrm{H}})\left(\mathbf{w}_{\mathrm{c}}\mathbf{w}_{\mathrm{c}}^{(i),\mathrm{H}}+\mathbf{w}_{\mathrm{c}}^{(i)}\mathbf{w}_{\mathrm{c}}^{\mathrm{H}}-\mathbf{w}_{\mathrm{c}}^{(i)}\mathbf{w}_{\mathrm{c}}^{(i),\mathrm{H}}\right)(\tilde{\mathbf{g}}_d^{DL}+\Delta\mathbf{g}_d^{DL})=(\Delta\mathbf{g}_d^{DL})^{\mathrm{H}}\left(2\,\mathrm{Re}\left\{\mathbf{w}_{\mathrm{c}}\mathbf{w}_{\mathrm{c}}^{(i),\mathrm{H}}\right\}-\mathbf{w}_{\mathrm{c}}^{(i)}\mathbf{w}_{\mathrm{c}}^{(i),\mathrm{H}}\right)\Delta\mathbf{g}_d^{DL}$$
$$+2\,\mathrm{Re}\left\{\tilde{\mathbf{g}}_d^{DL}\left(2\,\mathrm{Re}\left\{\mathbf{w}_{\mathrm{c}}\mathbf{w}_{\mathrm{c}}^{(i),\mathrm{H}}\right\}-\mathbf{w}_{\mathrm{c}}^{(i)}\mathbf{w}_{\mathrm{c}}^{(i),\mathrm{H}}\right)\Delta\mathbf{g}_d^{DL}\right\}+(\tilde{\mathbf{g}}_d^{DL})^{\mathrm{H}}\left(2\,\mathrm{Re}\left\{\mathbf{w}_{\mathrm{c}}\mathbf{w}_{\mathrm{c}}^{(i),\mathrm{H}}\right\}-\mathbf{w}_{k}^{(i)}\mathbf{w}_{\mathrm{c}}^{(i),\mathrm{H}}\right)\tilde{\mathbf{g}}_d^{DL}. \quad (37)$$

where Λ_m is the norm-bounded error matrix given as

$$\begin{aligned}&||\Lambda_m||\\&\leq||(\tilde{\mathbf{g}}_m^{UL})^{\mathrm{H}}\Delta\mathbf{g}_m^{UL}||+||(\Delta\mathbf{g}_m^{UL})^{\mathrm{H}}\tilde{\mathbf{g}}_m^{UL}||+||(\Delta\mathbf{g}_m^{UL})^{\mathrm{H}}\Delta\mathbf{g}_m^{UL}||,\\&\leq||(\tilde{\mathbf{g}}_m^{UL})^{\mathrm{H}}||\,||\Delta\mathbf{g}_m^{UL}||+||(\Delta\mathbf{g}_m^{UL})^{\mathrm{H}}||\,||\tilde{\mathbf{g}}_m^{UL}||+\\&\quad||(\Delta\mathbf{g}_m^{UL})^{\mathrm{H}}||\,||\Delta\mathbf{g}_m^{UL}||,\\&\leq\varepsilon_m^2+2\varepsilon_u||\tilde{\mathbf{g}}_m^{UL}||=\varsigma_m. \quad (50)\end{aligned}$$

Using (50), (31) and (34) are transformed with their lower bounds as

$$p_{u,j}^{UL}\mathbf{z}_u^{\mathrm{H}}\left((\tilde{\mathbf{g}}_u^{UL})^{\mathrm{H}}\tilde{\mathbf{g}}_u^{UL}+\varsigma_u\mathbf{I}\right)\mathbf{z}_u\leq\tilde{\lambda}_{u,j}^{UL},\forall m\in\mathcal{U} \quad (51)$$

$$\mu_{u,j}^{UL}\geq\sum_{(m,n)\in\mathcal{Q}_{u,j}}p_{m,n}^{UL}\mathbf{z}^{\mathrm{H}}\left((\tilde{\mathbf{g}}_m^{UL})^{\mathrm{H}}\tilde{\mathbf{g}}_m^{UL}+\varsigma_m\mathbf{I}\right)\mathbf{z}_m+P_{SI}+\sigma_{BS}^{UL^2}, \quad (52)$$

where

$$\tilde{\lambda}_{u,j}^{UL}=\lambda_{u,j}^{UL}(\mu_{u,j}^{UL})^{(i)}+(\lambda_{u,j}^{UL})^{(i)}\mu_{u,j}^{UL}-(\lambda_{u,j}^{UL})^{(i)}(\mu_{U,j}^{UL})^{(i)},$$

Denoting $\boldsymbol{\lambda}_{\mathrm{c}}=\{\lambda_{\mathrm{c},1}^{DL}\dots\lambda_{\mathrm{c},D}^{DL}\}$, $\boldsymbol{\lambda}_{\mathrm{p}}=\{\lambda_{\mathrm{p},1}^{DL}\dots\lambda_{\mathrm{p},D}^{DL}\}$, $\boldsymbol{\lambda}=\{\lambda_{1,1}^{UL}\dots\lambda_{J,D}^{UL}\}$, $\boldsymbol{\mu}_{\mathrm{c}}=\{\mu_{\mathrm{c},1}^{DL}\dots\mu_{\mathrm{c},D}^{DL}\}$, $\boldsymbol{\mu}_{\mathrm{p}}=\{\mu_{\mathrm{p},1}^{DL}\dots\mu_{\mathrm{p},D}^{DL}\}$, $\boldsymbol{\mu}=\{\mu_{1,1}^{UL}\dots\mu_{U,J}^{UL}\}$ and $\boldsymbol{\Phi}=\{\mathbf{w}_c,\mathbf{w},\mathbf{P},\mathbf{c},\boldsymbol{\lambda}_{\mathrm{c}},\boldsymbol{\lambda}_{\mathrm{p}},\boldsymbol{\lambda},\boldsymbol{\mu}_{\mathrm{c}},\boldsymbol{\mu}_{\mathrm{p}},\boldsymbol{\mu},\boldsymbol{\beta}_{\mathrm{c}},\boldsymbol{\beta}_{\mathrm{p}}\}$ and using the LMIs in (40), (41), (47) and (48) and the inequalities in (51) and (52), the problem (P3) is transformed as

$$(P4):\max_{\boldsymbol{\Phi}}\ OBJ \quad (53a)$$

$$\text{s.t. } (C.1),(C.3),(C.5),(40),(41),(47),(48),(51),(52), \quad (53b)$$

$$(C_2.2):\sum_{i\in\mathcal{D}}C_i\leq\log_2(1+\lambda_{\mathrm{c},d}^{DL}),\forall d\in\mathcal{D}, \quad (53c)$$

$$(C_2.4):C_d^{DL}+\log_2(1+\lambda_{\mathrm{p},d}^{DL})\geq R_{d,min}^{DL},\forall d\in\mathcal{D}, \quad (53d)$$

$$(C_2.6):\sum_{j\in\mathcal{J}}\log_2(1+\lambda_{u,j}^{UL})\geq R_{u,min}^{UL},\forall u\in\mathcal{U}, \quad (53e)$$

where OBJ is defines as

$$OBJ=\frac{(1-\chi)}{\xi_{SE}}\Big(\sum\nolimits_{d\in\mathcal{D}}(C_d^{DL}+\log_2(1+\lambda_{\mathrm{p},d}^{DL}))+\sum\nolimits_{u\in\mathcal{U}}\log_2(1+\lambda_{u,j}^{UL})\Big)-\frac{\chi}{\xi_{PT}}P_T. \quad (54)$$

Note that by solving (P4) optimally in an iterative manner, we can gradually improve the lower bound. Moreover, the objective function in (P4) increases monotonically, which ensures convergence to a stationary point. The trade-off parameter χ is adjusted to achieve the desired priority of the objective functions. $\chi=0$ is used to optimize the SE objective function, while χ_{EE} is used to optimize EE, which can be obtained from (27a) = 0. The optimal SE-EE trade-off problem

Algorithm 1 Proposed Algorithm

1: Initialize $\mathbf{w}_{\mathrm{c}}^{(i)}$, $\mathbf{w}^{(i)}$, $\mathbf{P}^{(i)}$, $\boldsymbol{\mu}_{\mathrm{c}}{}^{(i)}$, $\boldsymbol{\mu}_{\mathrm{p}}{}^{(i)}$, $\boldsymbol{\mu}_{u}{}^{(i)}$, $\chi^{(j)}$, j_{max}, i_{max} and $i=j=1$.
2: Evaluate ξ_{SE} and ξ_{PT}.
3: **while** $j\leq j_{max}$ **do**
4: **while** $i\leq i_{max}$ **do**
5: Evaluate $\mathbf{w}_{\mathrm{c}}^{(i+1)}$, $\mathbf{w}^{(i+1)}$, $\mathbf{P}^{(i+1)}$ using problem (P4)
6: Evaluate SE and EE using (15) and (17) respectively
7: $i\rightarrow i+1$
8: **end while**
9: Obtain $\chi^{(j+1)}=SE\xi_{PT}/(SE\xi_{PT}+EE\xi_{SE})$
10: $j\rightarrow j+1$
11: **end while**
12: **Output:** χ^*,$\mathbf{w}_{\mathrm{c}}^{(*)}$,$\mathbf{w}^{(*)}$, $\mathbf{P}^{(*)}$.

under the SCA framework is summarized in **Algorithm 1**. The step 1 of **Algorithm 1** indicates the initialization of auxiliary variables and iterations and the maximum number of iterations. In step 2, normalization parameters ξ_{SE} and ξ_{PT} are evaluated by maximizing the SE and minimizing the total power respectively. Using solver CVX, we obtain $\mathbf{w}_{\mathrm{c}}^{(i+1)}$, $\mathbf{w}^{(i+1)}$, $\mathbf{P}^{(i+1)}$ using problem (P4) in step 5. In step 6, SE and EE are evaluated at $\mathbf{w}_{\mathrm{c}}^{(i+1)}$, $\mathbf{w}^{(i+1)}$, $\mathbf{P}^{(i+1)}$ using (15) and (17) respecively. Update the inner iteration loop for the OBJ convergence in step 7. The trade-off parameter is updated in step 9. In step 10, the outer iteration loop is updated for the trade-off parameter convergence. Further, as evident from **Algorithm 1**, the computational complexity of step 5 is significantly higher than other steps that use SDP to obtain an optimal solution [52]. The number of arithmetic operations required to solve a standard real-valued SDP problem.

$$\min_{\mathbf{x}\in\mathcal{R}^n}\mathbf{c}^T\mathbf{x}\quad\text{s.t. }\mathbf{A}_0+\sum_{i=1}^{n}x_i\mathbf{A}_i\succeq\mathbf{0},\quad\|\mathbf{x}\|_2\leq R.$$

where $\mathbf{A}_i$ denotes the symmetric block-diagonal matrices with P diagonal blocks of size $a_l\times a_l, l=1,\dots,P$, is upper bounded by

$$\mathbb{D}=\mathcal{O}\left(\left(\sum_{i=1}^{I}d_i+2l\right)^{1/2}g\left(g^2+\underbrace{g\sum_{i=1}^{I}d_i^2+\sum_{i=1}^{I}d_i^3}_{\text{due to LMI}}\right)\right), \quad (55)$$

where $g=g_1+g_2$ in which g_1 and g_2 represents the number of variables $\mathbf{w}$ and $\mathbf{w}_{\mathrm{c}}$ given by $g_1=D*M_t$ and $g_2=M_t$

TABLE IV: Complexity analysis.

Variable	Dimension of block (d_i)
$\mathbf{w}$	$d_1 = M_t + 1$ $d_2 = M_t + D$
$\mathbf{w}_c$	$d_3 = M_t + 1$, $d_4 = M_t + D + 1$

TABLE V: Run time complexity.

DL users	UL users	Transmit antennas	Runtime complexity (sec)
3	2	5	872.34
3	2	2	577.12
5	2	5	1236.11
5	2	2	899.79
3	4	5	874.94
3	4	2	580.73
5	4	5	1245.59
5	4	2	903.23

respectively, and I represents the number of LMIs of size d_i given in Table IV.

The detailed running time complexity of the proposed algorithm is analyzed with the following system configuration: 2.90 GHz Intel(R) Core(TM) i7-10700 CPU with 40 GB RAM. For the different numbers of DL users, UL users, and transmit antennas the run-time complexity of the system is given in Table V, where we can observe that the runtime complexity is majorly influenced by the DL users and transmit antennas. This observation is also supported by the complexity analysis expression given in (55).

IV. Simulation Results

In this section, we show the effectiveness of the proposed FD-RSMA. Toward this, we use Monte Carlo simulations with over 100 independent realizations of randomly generated channels to evaluate the average performance and effectiveness of the proposed **Algorithm 1**. Additionally, we investigate the impact of RSMA on the overall performance of the network, comparing it to both SDMA and NOMA. For simulation, it is assumed that the BS has $M_t = 5$ transmit and $M_r = 8$ receive antennas and located at (0,60m). Moreover, we set D = 4 DL users, and U = 2 and assume that users are distributed randomly circularly symmetric Gaussian centered at $(x_{UL}, 0)$, $x_{UL} = 30$ m and $(x_{DL}, 0)$, $x_{DL} = 30$ m respectively, within a radius of $R_c = 30$ m [22]. The minimum rate for DL and UL users and the available transmit power at the BS and the UL users are set respectively as $R^{DL}_{d,min} = R^{DL}_{min} = 0.1$ and $R^{UL}_{u,min} = R^{UL}_{min} = 0.1$ and $p^{DL}_{max} = p_{max} = 40$ dBm and $p^{UL}_{u,max} = p^{UL}_{max} = 0$ dBm. The noise power is set as $\sigma^{UL^2}_{BS} = \sigma^{DL^2}_{d} = -74$ dBm, $\forall d$. Furthermore, the large-scale path-loss (in dB) is followed as $P_{L_i} = P_{L_0}(d_i/d_0)^{-\alpha_i}$, where $P_{L_0} = -30$ dB denotes the path-loss at the reference distance of d_0 = 1m, and α_i ($\forall i \in \mathbf{g}^{DL}_d, \mathbf{g}^{UL}_u, \mathbf{F}, h_{d,u}$) represents the path-loss exponent between the BS and the d-th DL user, the u-th UL user-BS, the SI channel, and the u-th UL user-d-th DL user links, respectively. Besides, d_i denotes the distance of the i^{th} link, and the path-loss exponents are assumed to be α_i = 2.2. We assume that all links' except the SI channel suffer from small-scale fading which follows the the Rayleigh distribution. The small-scale facing of the SI channel follows the Rician distribution. The norm bound of the imperfect channels are considered as $\varrho_d = \varepsilon_u = \varpi_{d,u} = \delta, \forall d \in \mathcal{D}$ and $u \in \mathcal{U}$.

The results of the trade-off analysis for the FD-RSMA system are presented in Fig. (2). In this analysis, the objective

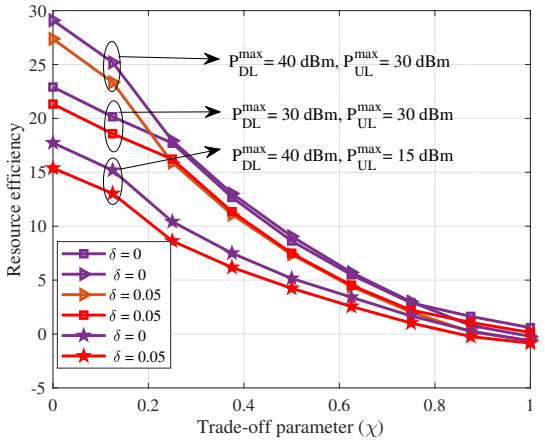

(a) Trade-off parameter (χ) vs Resource efficiency.

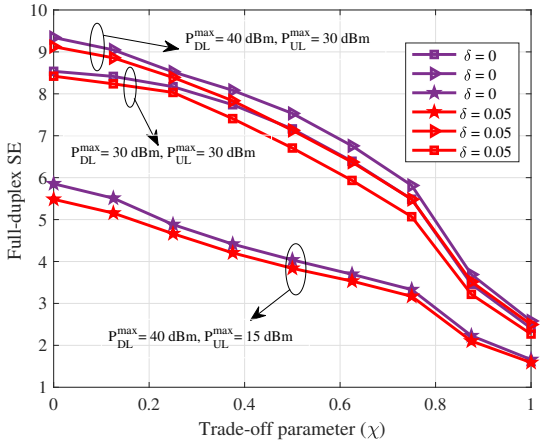

(b) Trade-off parameter (χ) vs Full-duplex SE.

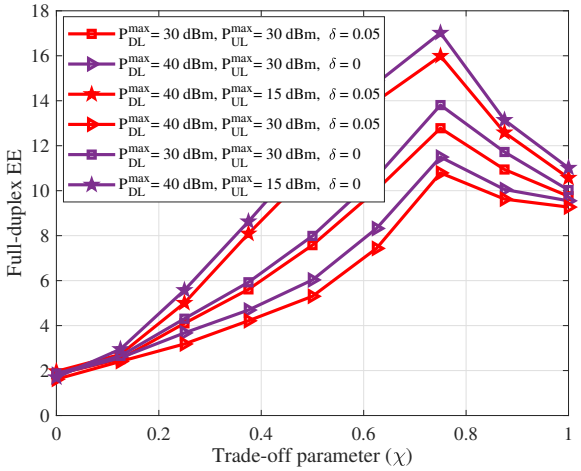

(c) Trade-off parameter (χ) vs Full-duplex EE.

Fig. 2: Trade-off analysis

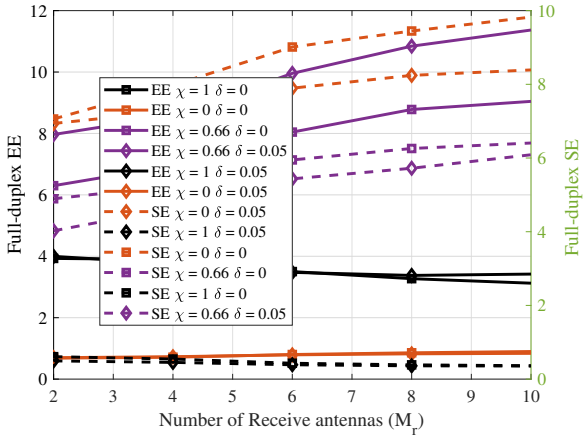

Fig. 3: Number of receive antenna (M_r) vs Full-duplex EE and SE.

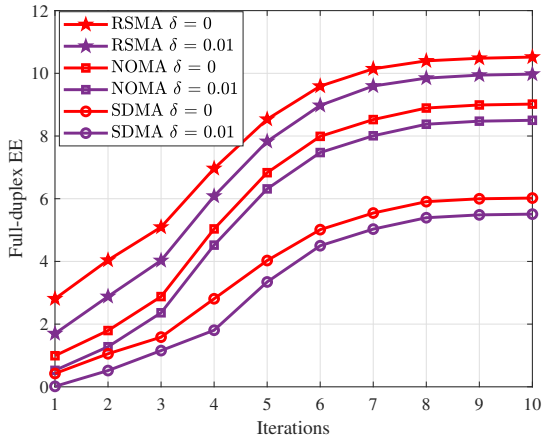

Fig. 4: System Convergence.

function of the SOO problem is referred to as resource efficiency (RE). Figs. (2a), (2b), and (2c) illustrate the influence of trade-off parameter χ on RE, full-duplex SE, and full-duplex EE, respectively, considering different UL and DL transmit powers for both perfect and imperfect CSI scenarios. The values of ξ_{PT} and ξ_{SE} in RE are set to the maximum total power consumption given by $p_{max}^{DL} + U * p_{max}^{UL} + PS$ and the minimum QoS required given by $D * R_{min}^{DL} + U * R_{min}^{UL}$ respectively. When $\chi = 0$, the focus is on maximizing SE, aiming to achieve maximum RE by harnessing the full potential of available transmit power. Consequently, at $\chi = 0$, we observe the maximum of full-duplex SE, accompanied by the minimum full-duplex EE. In contrast, when $\chi = 1$, the emphasis shifts to minimizing transmit power, utilizing only the necessary power to meet QoS requirements. This results in high EE but not necessarily at its maximum, and there is a corresponding decrease in SE. In both scenarios, there is a need to compromise between SE and EE, as maximizing one comes at the expense of the other. As χ increases from 0 to 1, the influence of the power minimization component becomes increasingly dominant, causing the BS to operate at lower power levels. This establishes an SE-EE trade-off: SE experiences a decline while EE sees an increase until the optimal χ is reached. At this optimal point, the maximum EE is achieved, accompanied by an improvement in SE. This trade-off highlights the inherent tension between maximizing SE and minimizing energy consumption in the considered FD-RSMA system. This behavior is evident in Figs. (2b) and (2c). Beyond the optimal χ, further increases result in decreased EE, SE, and RE. Furthermore, full-duplex SE for the perfect CSI is higher than the imperfect CSI. At $\chi = 1$, the impact of imperfections, P_{max}^{DL}, and P_{max}^{UL} on RE, EE, and SE diminish due to the power minimization problem.

The impact of the number of receive antennas (M_r) on the full duplex EE and full duplex SE for different trade-off parameters considering both perfect and imperfect CSI is shown in Fig. 3. We can observe that the increase in M_r increases both EE and SE due to enhanced diversity improving the signal reception. This leads to an increase in theUL rate, notably for the EE which is nearly optimal with $\chi = 0.66$ is higher than the $\chi = 0$ and $\chi = 1$. Because of rate maximization, the SE when $\chi = 0$ dominates compared to $\chi = 0$ and $\chi = 0.66$. Further increase in M_r causes the EE and SE to saturate. In addition, as expected, when perfect CSI is available, the EE and SE are always higher than the case when only imperfect CSI is available. As the number of receiving antennas increases, the impact of imperfect CSI is more noticeable in SE maximization cases due to the increased difficulty of estimating the channel. But, in near-optimal cases, the effect of imperfect CSI on SE decreases.

The convergence of the full-duplex EE using the optimal transmit and receive beamformers,UL power allocation, and trade-off parameter χ from algorithm 1 is shown in Fig. 4. FD-RSMA is compared with FD-NOMA and FD-SDMA with perfect and imperfect CSI with the latter used as a benchmark scheme. Here, the normalizing parameters ξ_{PT} and ξ_{SE} are obtained by minimizing power and maximizing full-duplex SE problems respectively while satisfying the corresponding QoS constraints. Using the ξ_{PT} and ξ_{SE}, full-duplex EE is obtained for the optimal χ by updating it iteratively using step 9 of algorithm 1. In all the cases, the optimal EE is achieved after 8 iterations. FD-RSMA outperforms FD-NOMA and FD-SDMA by 76.04 % and 16.93 % respectively due to better interference management. Furthermore, full-duplex EE for the perfect CSI is higher than the imperfect CSI in all three schemes.

In Fig. 5, the relationship between full-duplex EE and full-duplex SE, and P_{max}^{UL} for different P_{max}^{DL} is illustrated. At each P_{max}^{UL}, the full-duplex EE and SE are determined using optimal transmit and receive beamformers,UL power allocation, and the trade-off parameter χ. As P_{max}^{UL} increases, the trade-off parameter χ decreases, signaling a shift towards maximizing full-duplex SE. This transition leads to a rise in overall transmit power, subsequently causing a reduction in full-duplex EE. The total transmit power increases until it satisfies the QoS constraint, plateauing for further increases in P_{max}^{UL} and resulting in saturation in full-duplex SE and EE. At a higher norm bounded error $\delta = 0.05$, the decrease in full-duplex EE is more pronounced than the decrease in SE. This discrepancy arises because, at higher δ, the BS utilizes more power to achieve a better EE-SE trade-off. At elevated

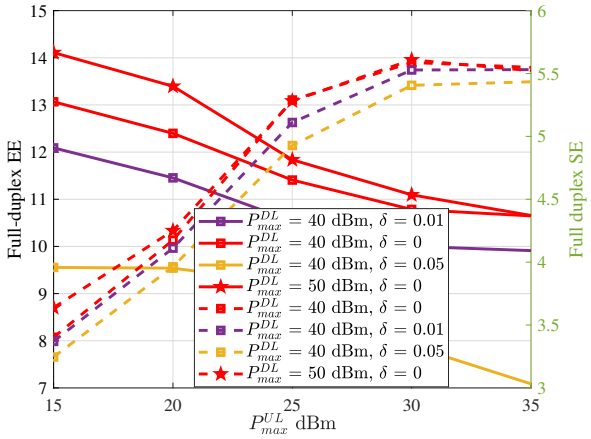

Fig. 5: UL transmit power (P^{UL}_{max}) vs Full-duplex EE and SE.

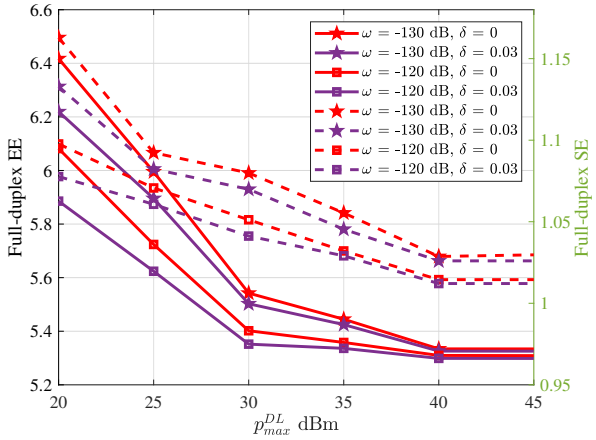

Fig. 6: DL transmit power (P^{DL}_{max}) vs Full-duplex EE and SE.

values of P^{UL}_{max}, optimal χ is crucial for the BS to employ limited transmit power, minimizing the impact of P^{DL}_{max} on full-duplex EE.

Fig. 6 illustrates the dependence of full-duplex EE and full-duplex SE on the DL power P^{DL}_{max} for various RSI (ω) scenarios, considering both perfect and imperfect conditions. At each P^{DL}_{max}, the optimal transmit and receive beamformers,UL power allocation, and trade-off parameter χ are employed to obtain the full-duplex EE and SE. As P^{DL}_{max} increases, the optimal χ decreases, resulting in an increase in DL transmit power. This, in turn, causes a decrease in full-duplex SE and leads to a reduction in full-duplex EE until the QoS constraint is reached. Beyond this point, further increases in P^{DL}_{max} result in minimal changes to both full-duplex SE and EE. Additionally, an increase in the RSI coefficient from -130 dB to -120 dB is observed to lead to a decrease in both full-duplex SE and EE. At higher values of P^{DL}_{max}, achieving a better EE-SE trade-off involves optimizing χ to encourage the BS to use limited transmit power. This strategy minimizes the impact of imperfections, ω and P^{DL}_{max} on both full-duplex spectral SE and EE.

V. Conclusion

This paper studied RSMA-Integrated FD communications with the objective of achieving a better understanding of the EE and SE trade-offs. In particular, we formulated the MOO problem to maximize SE and EE to optimize the transmit and receiver beamformers at the BS as well as power allocation at the ULs under imperfect CSI conditions in order to optimize the transmit and receiver beamformers. The formulated problem was reformulated to the SOO problem using a weighted sum approach. Next, we proposed an iterative algorithm based on the SCA scheme using the generalized S-procedure to achieve a near-optimal solution. Monte Carlo simulations are used to show the impact of trade-off parameter on the SOO function, FD SE, and EE with perfect and imperfect CSI. The dependency ofUL transmit power on FD EE and SE for different DL transmit powers and the dependency of DL transmit power on FD EE and FD SE for different residual self-interference was presented. The simulation results show that FD-RSMA is outperforms both FD-NOMA and FD-SDMA by 16.93 % and 76.04 % respectively due to better interference management. Finally, it is anticipated that the analysis, algorithms, and simulation results presented in this paper will find application in future wireless networks where FD communications and RSMA will be expected to play a pivotal role in delivering high SE while improving EE.

References

[1] G. P. Fettweis and H. Boche, "6G: The personal tactile internet—and open questions for information theory," *IEEE BITS Inf. Theory Mag.*, vol. 1, no. 1, pp. 71–82, Sep. 2021.

[2] H. Zheng, K. Xiong, P. Fan, Z. Zhong, and K. B. Letaief, "Wireless network design for intelligent services: From an age-energy efficiency perspective," *IEEE Network*, vol. 38, no. 3, pp. 244–253, May 2024.

[3] J. Tang, D. K. C. So, E. Alsusa, and K. A. Hamdi, "Resource efficiency: A new paradigm on energy efficiency and spectral efficiency tradeoff," *IEEE Trans. Wireless Commun.*, vol. 13, no. 8, pp. 4656–4669, Aug. 2014.

[4] S. He, Y. Huang, Y. Lu, C. Qi, and L. Yang, "Resource efficiency: A new beamforming design for multicell multiuser systems," *IEEE Trans. Veh. Technol.*, vol. 65, no. 8, pp. 6063–6074, Aug. 2016.

[5] H. Harada, K. Mizutani, T. Matsumura, T. Kato, and K. Shioiri, "Development of full-duplex cellular system for beyond 5G and 6G systems," in *Proc. PIMRC*, Sep. 2022, pp. 01–05.

[6] M. Katwe, K. Singh, B. Clerckx, and C.-P. Li, "Rate-splitting multiple access and dynamic user clustering for sum-rate maximization in multiple RISs-aided uplink mmWave system," *IEEE Trans. Commun*, vol. 70, no. 11, pp. 7365–7383, Nov. 2022.

[7] ——, "Rate splitting multiple access for sum-rate maximization in IRS aided uplink communications," *IEEE Trans. Wireless Commun.*, vol. 22, no. 4, pp. 2246–2261, Apr. 2023.

[8] D. Yu, J. Kim, and S.-H. Park, "An efficient rate-splitting multiple access scheme for the downlink of C-RAN systems," *IEEE Wireless Commun. Lett.*, vol. 8, no. 6, pp. 1555–1558, Dec. 2019.

[9] S. Pala, M. Katwe, K. Singh, B. Clerckx, and C.-P. Li, "Spectral-efficient RIS-aided RSMA URLLC: Toward mobile broadband reliable low latency communication (mBRLLC) system," *IEEE Trans. Wireless Commun.*, vol. 23, no. 4, pp. 3507–3524, Apr. 2024.

[10] S. Naser, P. C. Sofotasios, L. Bariah, W. Jaafar, S. Muhaidat, M. Al-Qutayri, and O. A. Dobre, "Rate-splitting multiple access: Unifying NOMA and SDMA in MISO VLC channels," *IEEE Open J. Veh. Technol.*, vol. 1, pp. 393–413, Oct. 2020.

[11] M. Katwe, K. Singh, C.-P. Li, S. Prakriya, B. Clerckx, and G. K. Karagiannidis, "Enhanced user fairness and performance for eMBB-URLLC uplink traffic with rate-splitting based super-positioning," *IEEE Trans. Wireless Commun.*, pp. 1–1, May 2024.

[12] D. Nguyen, L.-N. Tran, P. Pirinen, and M. Latva-aho, "On the spectral efficiency of full-duplex small cell wireless systems," *IEEE Trans. Wireless Commun.*, vol. 13, no. 9, pp. 4896–4910, 2014.

[13] S. Pala, M. Katwe, K. Singh, T. A. Tsiftsis, and C.-P. Li, "Robust transmission design for RIS-aided full-duplex-rsma V2X communications via multi-agent DRL," *IEEE Trans. Veh. Technol.*, vol. Early access, pp. 1–15, Sep. 2024.

[14] M. Katwe, K. Singh, P. K. Sharma, C.-P. Li, and Z. Ding, "Dynamic user clustering and optimal power allocation in UAV-assisted full-duplex hybrid NOMA system," *IEEE Trans. Wireless Commun.*, vol. 21, no. 4, pp. 2573–2590, Nov. 2022.

[15] A. Kilzi, J. Farah, C. A. Nour, and C. Douillard, "Optimal resource allocation for full-duplex IoT systems underlaying cellular networks with mutual SIC NOMA," *IEEE Internet Things J.*, vol. 8, no. 24, pp. 17 705–17 723, Dec 2021.

[16] J. Ma, C. Huang, and Q. Li, "Energy efficiency of full- and half-duplex decode-and-forward relay channels," *IEEE Internet Things J.*, vol. 9, no. 12, pp. 9730–9748, Jun. 2022.

[17] Y. Mao, B. Clerckx, and V. O. Li, "Energy efficiency of rate-splitting multiple access, and performance benefits over SDMA and NOMA," in *proc. ISWCS*, Aug. 2018, pp. 1–5.

[18] I. Abu Mahady, E. Bedeer, S. Ikki, and H. Yanikomeroglu, "Energy efficiency maximization of full-duplex NOMA systems with improper Gaussian signaling under imperfect self-interference cancellation," *IEEE Commun. Lett.*, vol. 26, no. 7, pp. 1613–1617, Jul. 2022.

[19] M. Katwe, K. Singh, P. K. Sharma, and C.-P. Li, "Energy efficiency maximization for UAV-assisted full-duplex NOMA system: User clustering and resource allocation," *IEEE Trans. Green Commun. Netw.*, vol. 6, no. 2, pp. 992–1008, Jun. 2022.

[20] H. Chen, G. Li, and J. Cai, "Spectral–energy efficiency tradeoff in full-duplex two-way relay networks," *IEEE Syst J.*, vol. 12, no. 1, pp. 583–592, Mar. 2018.

[21] D. Wen, G. Yu, R. Li, Y. Chen, and G. Y. Li, "Results on energy- and spectral-efficiency tradeoff in cellular networks with full-duplex enabled base stations," *IEEE Trans. Wireless Commun.*, vol. 16, no. 3, pp. 1494–1507, Mar. 2017.

[22] K. Singh, K. Wang, S. Biswas, Z. Ding, F. A. Khan, and T. Ratnarajah, "Resource optimization in full duplex non-orthogonal multiple access systems," *IEEE Trans. Wireless Commun.*, vol. 18, no. 9, pp. 4312–4325, Sep. 2019.

[23] B. Clerckx, Y. Mao, R. Schober, and H. V. Poor, "Rate-splitting unifying SDMA, OMA, NOMA, and multicasting in MISO broadcast channel: A simple two-user rate analysis," *IEEE Wireless Commun. Lett.*, vol. 9, no. 3, pp. 349–353, Mar. 2020.

[24] B. Clerckx, Y. Mao, R. Schober, E. A. Jorswieck, D. J. Love, J. Yuan, L. Hanzo, G. Y. Li, E. G. Larsson, and G. Caire, "Is NOMA efficient in multi-antenna networks? a critical look at next generation multiple access techniques," *IEEE Open J. Commun. Soc.*, vol. 2, pp. 1310–1343, Jun. 2021.

[25] B. Clerckx, Y. Mao, E. A. Jorswieck, J. Yuan, D. J. Love, E. Erkip, and D. Niyato, "A primer on rate-splitting multiple access: Tutorial, myths, and frequently asked questions," *IEEE J. Sel. Areas Commun.*, pp. 1–1, Feb. 2023.

[26] J. Xu, O. Dizdar, and B. Clerckx, "Rate-splitting multiple access for short-packet uplink communications: A finite blocklength analysis," *IEEE Commun. Lett.*, vol. 27, no. 2, pp. 517–521, Feb 2023.

[27] Z. Yang, M. Chen, W. Saad, W. Xu, and M. Shikh-Bahaei, "Sum-rate maximization of uplink rate splitting multiple access (RSMA) communication," *IEEE Trans Mob Comput* ., vol. 21, no. 7, pp. 2596–2609, Jul. 2022.

[28] Z. Yang, M. Chen, W. Saad, and M. Shikh-Bahaei, "Optimization of rate allocation and power control for rate splitting multiple access (RSMA)," *IEEE Trans. Commun*, vol. 69, no. 9, pp. 5988–6002, Sep. 2021.

[29] Y. Mao, E. Piovano, and B. Clerckx, "Rate-splitting multiple access for overloaded cellular internet of things," *IEEE Trans. Commun.*, vol. 69, no. 7, pp. 4504–4519, Jul. 2021.

[30] Z. Lin, M. Lin, B. Champagne, W.-P. Zhu, and N. Al-Dhahir, "Secure and energy efficient transmission for RSMA-based cognitive satellite-terrestrial networks," *IEEE Wireless Commun. Lett.*, vol. 10, no. 2, pp. 251–255, Feb 2021.

[31] H. Kong, M. Lin, Z. Wang, J.-Y. Wang, W.-P. Zhu, and J. Wang, "Combined robust beamforming with uplink RSMA for multibeam satellite systems," *IEEE Trans. Veh. Technol.*, vol. 71, no. 9, pp. 10 167–10 172, Sep. 2022.

[32] B. Matthiesen, Y. Mao, A. Dekorsy, P. Popovski, and B. Clerckx, "Globally optimal spectrum- and energy-efficient beamforming for rate splitting multiple access," *IEEE Trans. Signal Process.*, vol. 70, pp. 5025–5040, Oct. 2022.

[33] H. M. Al-Obiedollah, K. Cumanan, J. Thiyagalingam, J. Tang, A. G. Burr, Z. Ding, and O. A. Dobre, "Spectral-energy efficiency trade-off-based beamforming design for MISO non-orthogonal multiple access systems," *IEEE Trans. Wireless Commun.*, vol. 19, no. 10, pp. 6593–6606, Oct. 2020.

[34] O. Amin, E. Bedeer, M. H. Ahmed, and O. A. Dobre, "Energy efficiency–spectral efficiency tradeoff: A multiobjective optimization approach," *IEEE Trans. Veh. Technol.*, vol. 65, no. 4, pp. 1975–1981, Apr. 2016.

[35] L. Deng, Y. Rui, P. Cheng, J. Zhang, Q. T. Zhang, and M. Li, "A unified energy efficiency and spectral efficiency tradeoff metric in wireless networks," *IEEE Commun. Lett.*, vol. 17, no. 1, pp. 55–58, Jan. 2013.

[36] Y. Hao, Q. Ni, H. Li, and S. Hou, "Robust multi-objective optimization for ee-se tradeoff in d2d communications underlaying heterogeneous networks," *IEEE Trans. Commun.*, vol. 66, no. 10, pp. 4936–4949, Oct. 2018.

[37] W. Wang, L. Gao, R. Ding, J. Lei, L. You, C. A. Chan, and X. Gao, "Resource efficiency optimization for robust beamforming in multi-beam satellite communications," *IEEE Trans. Veh. Technol.*, vol. 70, no. 7, pp. 6958–6968, Jul. 2021.

[38] S. Kurma, M. Katwe, K. Singh, T. Q. Duong, and C.-P. Li, "Spectral-energy efficient resource allocation in RIS-aided FD-MIMO systems," *IEEE Trans. Wireless Commun.*, vol. 23, no. 5, pp. 5125–5141, May 2024.

[39] G. Zhou, Y. Mao, and B. Clerckx, "Rate-splitting multiple access for multi-antenna downlink communication systems: Spectral and energy efficiency tradeoff," *IEEE Trans. Wireless Commun.*, vol. 21, no. 7, pp. 4816–4828, Jul. 2022.

[40] J. Hu, C. Sun, J. Wang, X. Gao, L. Xia, and Q. Wang, "Resource efficient and robust RSMA for visible light communications," *IEEE Photonics J.*, pp. 1–12, Apr. 2024.

[41] S. Poornima and A. V. Babu, "Power adaptation for enhancing spectral efficiency and energy efficiency in multi-hop full duplex cognitive wireless relay networks," *IEEE Trans. Mobile Comput.*, vol. 21, no. 6, pp. 2143–2157, Jun. 2022.

[42] H. V. Nguyen, V.-D. Nguyen, O. A. Dobre, S. K. Sharma, S. Chatzinotas, B. Ottersten, and O.-S. Shin, "On the spectral and energy efficiencies of full-duplex cell-free massive mimo," *IEEE J. Sel. Areas Commun.*, vol. 38, no. 8, pp. 1698–1718, Aug 2020.

[43] S. Khisa, M. Almekhlafi, M. Elhattab, and C. Assi, "Full duplex cooperative rate splitting multiple access for a MISO broadcast channel with two users," *IEEE Commun. Lett.*, vol. 26, no. 8, pp. 1913–1917, Aug. 2022.

[44] R. Allu, M. Katwe, K. Singh, T. Q. Duong, and C.-P. Li, "RSMA-integrated full-duplex communications for better energy and spectral-efficiency trade-off," in *Proc. Globecom Workshops*, Dec. 2023, pp. 1213–1218.

[45] ——, "Robust energy efficient beamforming design for ISAC full-duplex communication systems," *IEEE Wireless Communications Letters*, vol. Early access, pp. 1–1, 2024.

[46] M. Katwe, K. Singh, B. Clerckx, and C.-P. Li, "Improved spectral efficiency in STAR-RIS aided uplink communication using rate splitting multiple access," *IEEE Trans. Wireless Commun.*, vol. 22, no. 8, pp. 5365–5382, Aug. 2023.

[47] R. Allu, O. Taghizadeh, S. K. Singh, K. Singh, and C.-P. Li, "Robust beamformer design in active RIS-assisted multiuser MIMO cognitive radio networks," *IEEE Trans. Cogn. Commun. Netw.*, vol. 9, no. 2, pp. 398–413, Apr. 2023.

[48] Y. Sun, D. W. K. Ng, J. Zhu, and R. Schober, "Robust and secure resource allocation for full-duplex MISO multicarrier NOMA systems," *IEEE Trans. Commun*, vol. 66, no. 9, pp. 4119–4137, Sep. 2018.

[49] A. Khalili, S. Zargari, Q. Wu, D. W. K. Ng, and R. Zhang, "Multi-objective resource allocation for IRS-aided SWIPT," *IEEE Wireless Commun. Lett.*, vol. 10, no. 6, pp. 1324–1328, Jun. 2021.

[50] E. A. Gharavol and E. G. Larsson, "The sign-definiteness lemma and its applications to robust transceiver optimization for multiuser MIMO systems," *IEEE Trans. Signal Process*, vol. 61, no. 2, pp. 238–252, Oct. 2013.

[51] S. Boyd and L.Vandenberghe, *Convex Optimization*. NewYork, NY, USA: Cambridge Univ. Press, 2004.

[52] V. Radhakrishnan, O. Taghizadeh, and R. Mathar, "Hardware impairments-aware transceiver design for multi-carrier full-duplex MIMO relaying," *IEEE Trans. Veh. Technol.*, vol. 70, no. 2, pp. 1109–1121, Feb 2021.